# Transport Theory and Statistical Physics

## Subcell balance methods for radiative transfer on arbitrary grids

Marvin L. Adams [a]

[a] Texas A&M University College Station , TX, 77843-3
mladams@tamu.edu
Published online: 20 Nov 2006.

PLEASE SCROLL DOWN FOR ARTICLE

# SUBCELL BALANCE METHODS
# FOR RADIATIVE TRANSFER ON ARBITRARY GRIDS

Marvin L. Adams

Texas A&M University
College Station, TX 77843-3133
mladams@tamu.edu

## ABSTRACT

We present a new spatial discretization method. which enforces conservation on quadrilateral subcells in an arbitrarily connected grid of polygonal cells, for two-dimensional radiative transfer problems. We review what is known about the performance of existing methods for optically thick, diffusive regions of radiative transfer problems, focusing in particular on bilinear discontinuous (BLD) finite-element methods and the simple corner-balance (SCB) method. We discuss the close relation of the SCB and BLD methods, and how they differ. By careful analysis, we relate specific properties of the SCB solution to specific approximations in the SCB method. We then build our new method by discarding those SCB approximations that lead to undesirable properties and carefully constructing new approximations designed to yield more desirable properties. We compare BLD, SCB. and the new scheme on a series of test problems in slab and XY geometries; numerical results invariably agree with predictions of the analysis. The new method matches SCB in thick diffusive regions, as it was designed to, but vastly outperforms SCB given cells of fine and intermediate optical thickness, where it achieves results comparable to BLD.

## I. INTRODUCTION

General multi-dimensional radiative-transfer problems have many features that make them extremely difficult to solve computationally. In this paper we

present a method for solving such problems on arbitrary spatial grids. The method is based on enforcing energy conservation, or "balance," on subcells that we call "corners;" hence, we call our scheme a "corner-balance" (CB) method. Along with the exact balance equations we must devise approximate equations that relate surface- and volume-averaged unknowns, thus closing the system. We have created closure equations that allow the equations to be solved one subcell at a time, with no matrix inversions, when the total source in each subcell is given. That is, for purposes of sweeping the mesh during a given iteration, the method is strictly "upstream." We therefore call it an "upstream corner-balance" (UCB) method. We show here, by asymptotic analysis and numerical testing, that this UCB method is remarkably robust and accurate when applied to optically thick radiative-transfer problems.

Computational radiative transfer problems of practical interest often contain regions that are extremely optically thick in frequency ranges that contain a substantial portion of the radiant energy. Typically in such regions the dominant physical process is absorption and re-emission. Such regions are "diffusive" in the sense that the transport solution satisfies, to leading order, a diffusion equation.[1] If we apply a numerical transport method to such problems we would hope that in these thick diffusive regions the discrete transport solution would satisfy, to leading order, a discretized diffusion equation. If so, and if the diffusion discretization is accurate and has accurate boundary conditions, then our numerical transport solution is an accurate approximation of the exact solution in thick diffusive regions.

Powerful asymptotic analysis techniques have been developed in recent years for studying the behavior of numerical transport solutions in thick diffusive regions.[2-9] These analyses precisely reveal the equations satisfied by leading-order numerical solutions in such regions. In this paper we use an asymptotic analysis to study our UCB method, showing that it has very desirable properties but that under certain conditions its solution can degrade. We also study the method with a series of numerical tests, invariably finding that the predictions of the analysis are exactly correct.

In this paper we focus on the numerical solution of the following radiative-transfer equations on a very general spatial grid:[10]

$$\frac{1}{c}\frac{\partial \psi}{\partial t} + \bar{\Omega} \cdot \bar{\nabla} \psi + \sigma_a\left(\bar{r}, v, T(\bar{r}, t)\right) \psi\left(\bar{r}, v, \bar{\Omega}, t\right)$$

$$= \sigma_a\left(\bar{r}, v, T(\bar{r}, t)\right) B\left(v, T(\bar{r}, t)\right), \quad \bar{r} \in V, \tag{1a}$$

$$\psi\left(\bar{r}_s, v, \bar{\Omega}, t\right) = \psi_{inc}\left(\bar{r}_s, v, \bar{\Omega}, t\right) = \text{known}, \quad \bar{r}_s \in \partial V, \quad \bar{n}(\bar{r}_s) \cdot \bar{\Omega} < 0, \tag{1b}$$

$$\psi\left(\bar{r}, v, \bar{\Omega}, t\right)\Big|_{t=0} = I\left(\bar{r}, v, \bar{\Omega}\right) = \text{known}, \tag{1c}$$

$$C_p \frac{\partial T}{\partial t} = \int_0^\infty dv \int_{4\pi} d\Omega \, \sigma_a\left(\bar{r}, v, T\right)\left[\psi\left(\bar{r}, v, \bar{\Omega}, t\right) - B(v, T)\right] + Q(\bar{r}, t), \tag{2a}$$

$$T(\bar{r}, t)\Big|_{t=0} = T_0(\bar{r}) = \text{known}. \tag{2b}$$

If a numerical method is to handle this difficult problem, it must be able to handle a simpler problem that has only one frequency group. If we consider such a one-group problem and employ standard time-differencing techniques, we find that during each time step we must solve the following steady-state transport problem:

$$\bar{\Omega} \cdot \bar{\nabla} \psi + \sigma_t(\bar{r}) \psi\left(\bar{r}, \bar{\Omega}\right) = \frac{1}{4\pi}\left[\sigma_t(\bar{r}) - \sigma_r(\bar{r})\right]\phi(\bar{r}) + S\left(\bar{r}, \bar{\Omega}\right), \quad \bar{r} \in V, \tag{3a}$$

$$\psi\left(\bar{r}_s, \bar{\Omega}\right) = \psi_{inc}\left(\bar{r}_s, \bar{\Omega}\right), \quad \bar{r}_s \in \partial V, \quad \bar{n}(\bar{r}_s) \cdot \bar{\Omega} < 0, \tag{3b}$$

where

$$\phi(\bar{r}) = \int_{4\pi} d\Omega \, \psi\left(\bar{r}, \bar{\Omega}\right), \tag{4}$$

$$\sigma_t(\bar{r}) = \sigma_a(\bar{r}) + \frac{1}{c\Delta t}, \quad \text{if implicit time differencing,} \tag{5a}$$

$$\sigma_r(\bar{r}) \quad \text{and} \quad S(\bar{r}, \bar{\Omega}) \quad \text{depend on details of time differencing.} \tag{5b}$$

In this paper we focus on the computational solution of this one-group steady-state problem. The limit of interest is characterized by an optically thick domain with small $S$ and with $\sigma_r \ll \sigma_t$.

Setting the stage for our work, we shall review in the following section a well-known analysis of the exact transport solution in an asymptotic limit that corresponds to an optically thick region with $\sigma_r \ll \sigma_t$. This shows that the exact solution, to leading-order, satisfies a simple diffusion equation. We discuss the behavior we would like a numerical transport solution to have in the same physical limit, and review what is known about the behavior of previously proposed numerical schemes. In Section III we derive a "simple" corner-balance

method, discuss its relationship to finite-element methods, and analyze its behavior in the optically thick diffusive limit. In Section IV we develop and analyze an "upstream" corner-balance method that permits subcell-by-subcell (as opposed to cell-by-cell) sweeping of an arbitrary grid. This method is based on SCB but is designed to be far more accurate given cells of fine and intermediate optical thickness. We briefly discuss iterative acceleration in Section V, then present numerical results in Section VI. The final section is devoted to a summary and some concluding remarks.

## II. REVIEW OF KNOWN RESULTS

### A. Asymptotic Analysis of Exact Solution

A brief review of the behavior of the exact transport solution in a diffusive region is now in order. This review is taken from reference 11 and references therein. We begin by considering a "scaled" version of the transport equation:

$$\bar{\Omega} \cdot \bar{\nabla} \psi + \frac{\sigma_t(\bar{r})}{\varepsilon} \psi(\bar{r}, \bar{\Omega}) = \frac{1}{4\pi} \left[ \frac{\sigma_t(\bar{r})}{\varepsilon} - \varepsilon \sigma_r(\bar{r}) \right] \phi(\bar{r}) + S(\bar{r}, \bar{\Omega}), \quad \bar{r} \in V, \quad (6a)$$

$$\phi(\bar{r}) = \int_{4\pi} d\Omega \, \psi(\bar{r}, \bar{\Omega}), \quad (6b)$$

$$\psi(\bar{r}_s, \bar{\Omega}) = \psi_{inc}(\bar{r}_s, \bar{\Omega}), \quad \bar{r}_s \in \partial V, \quad \bar{n}(\bar{r}_s) \cdot \bar{\Omega} < 0. \quad (6c)$$

Here $\varepsilon$ is a small parameter that determines the extent to which the problem is diffusive: the smaller $\varepsilon$ becomes, the more optically thick and highly scattering the problem becomes.

Next, we guess that the solution is a power series in $\varepsilon$, that is, we postulate

$$\psi = \psi^{(0)} + \varepsilon \psi^{(1)} + \varepsilon^2 \psi^{(2)} + \cdots \quad (7)$$

We then find that in the *interior* of the domain $V$ (that is, away from boundaries), the leading-order angular flux is isotropic and satisfies a diffusion equation:

$$\psi^{(0)}(\bar{r}, \bar{\Omega}) = \frac{1}{4\pi} \phi^{(0)}(\bar{r}), \quad (8a)$$

$$-\bar{\nabla} \cdot \frac{1}{3\sigma(\bar{r})} \bar{\nabla} \phi^{(0)} + \sigma_r(\bar{r}) \phi^{(0)}(\bar{r}) = S_0(\bar{r}), \qquad S_0(\bar{r}) = \int_{4\pi} d\Omega \, S(\bar{r}, \bar{\Omega}). \quad (8b)$$

Of course, this does not fully describe the leading-order interior solution, for the solution of the diffusion equation is not unique until it is subjected to

appropriate boundary conditions. One finds after considerable analysis that the boundary condition that gives the correct leading-order interior solution is:

$$\phi^{(0)}(\vec{r}_s) = 2 \int_{\vec{n}\cdot\vec{\Omega}<0} d\Omega\, W\left(\left|\vec{n}\cdot\vec{\Omega}\right|\right)\psi_{inc}(\vec{r}_s,\vec{\Omega})\ ,\ \vec{r}_s \in \partial V. \qquad (9)$$

Here $W$ is defined in terms of Chandrasekhar's $H$-function[12] for a purely scattering medium. but is reasonably well approximated by a simple polynomial:

$$2W(\mu) \approx \sqrt{3}\mu H(\mu) = 1.82\mu + 3.27\mu^2 \pm a\ few\ \% \approx 2\mu + 3\mu^2\ . \qquad (10)$$

Let us note two things about the boundary condition satisfied by the exact leading-order interior solution:

- It is a Dirchlét condition, specifying the energy density on the boundary.

- It retains no memory of *azimuthal* variations (about the surface normal) in the incident angular flux.

## B. Behavior of Existing Methods

Diffusion-limit analyses such as the one outlined above tell us a great deal about the exact transport solution in an optically thick region with $\sigma_r << \sigma_t$:

- Away from boundary layers, the leading-order solution is isotropic and satisfies a simple diffusion equation.

- Close to boundaries (within a few mean-free paths), the leading-order solution is more complicated, transitioning from full angular dependence to isotropy.

- The interior solution, which is diffusive, is partially determined by a boundary condition. This boundary condition is known. It is a Dirichlét condition given by a certain weighted integral of the incident intensity.

From this knowledge we can deduce many properties that we would like for a *numerical* transport solution to possess if the numerical method were applied to the same kind of problem:

- The leading-order numerical solution should be isotropic in the interior.

- The leading-order numerical solution should be smooth, as diffusion solutions are.

- The leading-order numerical solution in the interior should satisfy an accurate discretization of the same diffusion problem that the leading-order exact solution satisfies. This includes the Dirichlét boundary condition of Eqs. (9) and (10).

If a numerical transport solution can be shown to have these properties, then we can be confident that the method will be accurate for optically thick diffusive problems, even in the presence of unresolved boundary layers and even with very coarse spatial grids. This is quite a lot to ask of a numerical method, and it is not clear *a priori* that it is possible to achieve. The fundamental scale length in a transport problem is the mean-free path (defined to be $1/\sigma_t$), and traditional truncation-error analysis suggests that spatial cells should have optical thickness less than one mean-free path to guarantee an accurate numerical transport solution. In the physical limit of interest here, given any fixed spatial grid, the optical thickness of each cell tends toward infinity; thus, traditional logic seems to suggest that we seek an impossible goal. However, the fundamental scale length in a diffusion problem is the diffusion length (defined to be $[3\sigma_t \sigma_a]^{-1/2}$), which in the physical limit of interest here is much, much longer than a mean-free path. We have just seen that in this limit the analytic transport solution satisfies (to leading order in the interior) a diffusion problem. This offers hope: if a numerical transport solution satisfies a numerical *diffusion* discretization in this limit, then it has a chance to be accurate on a spatial grid that resolves only diffusion lengths – an extremely coarse grid in terms of mean-free paths.

A review of what is known about existing numerical transport methods in this limit is now in order, beginning with one-dimensional slab geometry. Larsen et al.[2,3,13] and Adams et al.[5,9] have shown that on a fixed spatial grid, as $\varepsilon \to 0$:

- The well-known diamond-difference method (DD) performs well in slab geometry if there are no unresolved boundary layers. Its leading-order solution has two additive components: one that satisfies a reasonable cell-edge differencing of the correct diffusion equation, and one that oscillates with $O(1)$ amplitude across the problem. The oscillating component is excited by any anisotropic intensity incident upon an optically thick spatial cell; it vanishes if incident intensities are all isotropic or if boundary layers are well resolved by the spatial grid.

- The linear discontinuous (LD) finite-element method (FEM) performs well in slab geometry even in problems that contain unresolved boundary layers. provided only that spatial cells are not larger than a diffusion length. Its robustness and the accuracy of its boundary condition both degrade if spatial cells get larger than a diffusion length. The LD method with mass-matrix lumping (the "lumped LD," or LLD method) is quite robust and always satisfies a boundary condition given by a $2\mu + 3\mu^2$ weighting of the incident intensity [see Eq. (10)].

- A "multiple-balance" method is robust and accurate, comparable to LLD.

- Balance-based characteristic methods behave exactly like discontinuous FEMs in thick diffusive problems. Thus, for example, the leading-order linear-moments (LM) solution is identical to the leading-order LD solution, which is quite good in most cases, as noted above.

- Most discontinuous finite-element methods (DFEMs) perform well in slab geometry, although it is possible to create DFEMs that fail. The "step" DFEM, which assumes the solution is constant in each cell, is an example of a DFEM that will fail in thick diffusive regions.

Researchers have recently learned how to analyze the diffusion-limit behavior of many methods in multidimensional settings. [5,9,14] In XY and XYZ geometries, we know that:

- Although they perform well on diffusive problems in slab geometry, unmodified DFEMs do not do as well in two and three dimensions. There are two classes of DFEMs: those that fail miserably, and those whose leading-order solutions satisfy discretizations of the correct diffusion problem. DFEMs in the latter class are not robust; they are susceptible to discontinuities, oscillations, negative solutions, and boundary conditions that are not good approximations to Eqs. (9) and (10).

- Mass-matrix lumping helps DFEMs in multidimensional problems, but not a great deal. Adams introduced[5] *surface-matrix* lumping, which further helps: when used in concert with mass-matrix lumping, it eliminates discontinuities in the leading-order

solution, mitigates oscillations, and improves the boundary condition. However, even with both kinds of lumping, DFEMs can still be plagued by oscillations and negative solutions, even on simple rectangular grids in XY geometry.

- On a rectangular grid in XY geometry, if one begins with the mass- and surface-matrix-lumped bilinear DFEM and *further* modifies it to make it as robust as LLD in slab geometry, the result is a method that can be interpreted as enforcing particle conservation on subcells and applying simple approximate closure relations.[15] That is, if one modifies the bilinear DFEM until it is robust, one obtains a simple corner-balance method (which we will describe in the next section). On a rectangular grid, this method is very robust: its solution is continuous, positive, and monotonic, and satisfies a boundary condition with a $2\mu + 3\mu^2$ weighting of the incident intensity, which is a very good approximation to the correct boundary condition [see Eq. (10)]. It is the precise two-dimensional analog of the LLD method in slab geometry. (Of course, the slab-geometry LLD method can also be viewed as a simple corner-balance method.)

- As we shall detail in this paper, corner-balance methods are easily developed for arbitrary spatial grids. Their accuracy for diffusive problems on such grids is one of the main topics we study here.

- As is true in slab geometry, balanced-based characteristics methods behave exactly like DFEMs in thick diffusive problems.[9] Thus, they either fail dramatically, or they are susceptible to discontinuities, oscillations, negative solutions, and inaccurate boundary conditions. To our knowledge, no one has yet attempted to modify characteristic methods to make them robust, in the way that the bilinear DFEM can be modified into the robust simple corner-balance scheme on rectangles.

To summarize, several methods perform quite well in slab geometry. The most robust of these satisfy subcell balance equations. In two and three dimensions, to our knowledge the only methods that are robust on rectangular grids are also based on subcell balance equations. In this paper we develop these methods, concentrating on their more computationally efficient "upstream" incarnations.

## III.    A "SIMPLE" CORNER-BALANCE METHOD

### A.  Derivation

Let us consider a two-dimensional spatial domain divided into polygonal cells. We shall not require that the polygons be convex; however, we require each polygon to have a point in its interior such that a line segment from that point to any vertex will remain entirely within the polygon. There is no restriction on the number of vertices a polygon can have or on the number of polygons that can meet at a point, but no pair of polygons can share more than one edge.

Once the problem domain is divided into polygonal cells, we subdivide each cell into subcells we call *corners*. Figure 1 depicts one such corner, labeled $c$, and the two neighboring corners ($c-1$ and $c+1$) it has in the same cell. The figure also defines the vectors $\vec{A}_{c\pm}$ and $\vec{B}_{c\pm}$, which are corner edge lengths multiplied by outward unit normals.

Now if we integrate the transport equation (3a) over corner $c$ we obtain:

$$\vec{\Omega}\cdot\left[\vec{A}_{c+}\psi_{c+} + \vec{A}_{c-}\psi_{c-} + \vec{B}_{c+}\psi_{c+1/2} + \vec{B}_{c-}\psi_{c-1/2}\right] + \sigma_{t,c}V_c\psi_c$$
$$= V_c\left(\frac{1}{4\pi}[\sigma_{tc} - \sigma_{rc}]\dot{\phi}_c + S_c\right), \tag{11}$$

where

$\quad V_c \quad = \quad$ the "volume" (actually area in 2D) of corner $c$;

$\quad \psi_c \quad = \quad$ intensity in direction $\vec{\Omega}$ averaged over corner $c$;

$\quad \psi_{c\pm1/2} \quad = \quad$ intensity in direction $\vec{\Omega}$ averaged over surface between $c$ and $c\pm1$;

$\quad \psi_{c\pm} \quad = \quad$ intensity in direction $\vec{\Omega}$ averaged over surface whose outward normal points along $\vec{A}_{c\pm}$.

Equation (11) is a conservation or "balance" equation for corner $c$. It contains no approximations. However, it contains five different averaged intensities: one in the corner and one on each corner surface. Thus, we require more equations if we are to close the system. For reasons we shall discuss later, we use a "step" closure on each corner surface that is also part of a *cell* surface. We choose a simple averaging closure on each corner surface that is *inside* a cell. The two closures are:
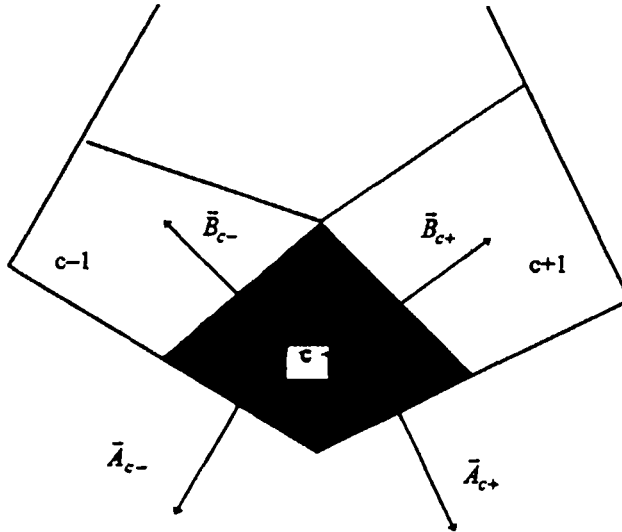
Figure 1. Corner $c$ and its neighboring corners ($c\pm1$) in a polygonal cell.

$$\psi_{c\pm} = \begin{cases} \psi_c, & \vec{A}_{c\pm} \cdot \vec{\Omega} > 0, \\ \psi_{c\pm}^{inc}, & \vec{A}_{c\pm} \cdot \vec{\Omega} < 0, \end{cases} \tag{12a}$$

$$\psi_{c\pm1/2} = \frac{1}{2}(\psi_c + \psi_{c\pm1}). \tag{12b}$$

We refer to Eqs. (11) and (12) as the "simple" corner-balance (SCB) method. The simplest angular discretization to use in conjunction with the SCB spatial discretization is the discrete-ordinates (commonly called "$S_N$") method, which replaces the integral in Eq. (4) with a quadrature sum. This gives:

$$\phi_c = \sum_{m=1}^{M} w_m \, \psi_c(\vec{\Omega}_m) = \sum_{m=1}^{M} w_m \, \psi_{m,c}, \tag{13}$$

which implies that Eqs. (11) and (12) need to be solved only for directions that are in the quadrature set; that is, only for $\vec{\Omega} = \vec{\Omega}_m$, $m=1,...,M$. We will henceforth use the subscript $m$ to denote an angular intensity in direction $\vec{\Omega}_m$.

Given a spatial grid of arbitrary polygons, the "simple" closure of Eq. (12b) can lead to a relatively complicated and expensive mesh-sweeping algorithm.

because it couples all the corner-averaged intensities in each polygonal cell. That is, once all the incident intensities and sources are known for an N-sided polygon, obtaining the corner-averaged intensities still requires the solution of an N×N matrix equation. While this might be acceptable on a grid of triangles or quadrilaterals, we would prefer to avoid it on a truly arbitrary grid. (It is tractable, but computationally costlier than we would prefer.) This is one motivation for developing an "upstream" corner balance method, which is the main focus of this paper.

## B.  Relation to Discontinuous Finite Elements

Let us consider for the moment a grid of rectangular cells in XY geometry. In this case the SCB method is fairly closely related to the bilinear discontinuous (BLD) finite-element method.[5,15] The standard BLD equation for the "southwest" intensity in the $ij$th rectangular cell is:

$$\frac{2}{3}\left[\frac{\psi_{m,ji}^{SW}+\psi_{m,ji}^{SE}}{2}-\psi_{m,i-1/2,j}^{S}\right]+\frac{1}{3}\left[\frac{\psi_{m,ij}^{NW}+\psi_{m,ji}^{NE}}{2}-\psi_{m,i-1/2,j}^{N}\right]+\frac{2}{3}\left[\frac{\psi_{m,ji}^{SW}+\psi_{m,ji}^{NW}}{2}-\psi_{m,i,j-1/2}^{W}\right]$$

$$+\frac{1}{3}\left[\frac{\psi_{m,ij}^{SE}+\psi_{m,ij}^{NE}}{2}-\psi_{m,i,j-1/2}^{E}\right]+\frac{(\sigma_t\Delta x\Delta y)_{ij}}{36}\left[4\psi_{m,ij}^{SW}+2\psi_{m,ij}^{SE}+\psi_{m,ij}^{NE}+2\psi_{m,ij}^{NW}\right]$$

$$=\frac{(\Delta x\Delta y)_{ij}}{36}\left[\begin{array}{l}4\big([\sigma_t-\sigma_r]\phi/4\pi+S\big)_{ij}^{SW}+2\big([\sigma_t-\sigma_r]\phi/4\pi+S\big)_{ij}^{SE}\\+\big([\sigma_t-\sigma_r]\phi/4\pi+S\big)_{ij}^{NE}+2\big([\sigma_t-\sigma_r]\phi/4\pi+S\big)_{ij}^{NW}\end{array}\right]. \qquad (14)$$

(See Figure 2 for notation.) There are similar equations centered in the other three corners.

If we employ mass-matrix lumping, Eq. (14) becomes

$$\frac{2}{3}\left[\frac{\psi_{m,ij}^{SW}+\psi_{m,ij}^{SE}}{2}-\psi_{m,i-1/2,j}^{S}\right]+\frac{1}{3}\left[\frac{\psi_{m,ij}^{NW}+\psi_{m,ij}^{NE}}{2}-\psi_{m,i-1/2,j}^{N}\right]$$

$$+\frac{2}{3}\left[\frac{\psi_{m,ij}^{SW}+\psi_{m,ij}^{NW}}{2}-\psi_{m,i,j-1/2}^{W}\right]+\frac{1}{3}\left[\frac{\psi_{m,ij}^{SE}+\psi_{m,ij}^{NE}}{2}-\psi_{m,i,j-1/2}^{E}\right] \qquad (15)$$

$$+\frac{(\sigma_t\Delta x\Delta y)_{ij}}{4}\psi_{m,ij}^{SW}=(\Delta x\Delta y)_{ij}\frac{1}{4}\big([\sigma_t-\sigma_r]\phi/4\pi+S\big)_{ij}^{SW}.$$

Note that the collision and source terms have become more *localized*, looking now like simple averages over the southwest corner. If we also try to localize the
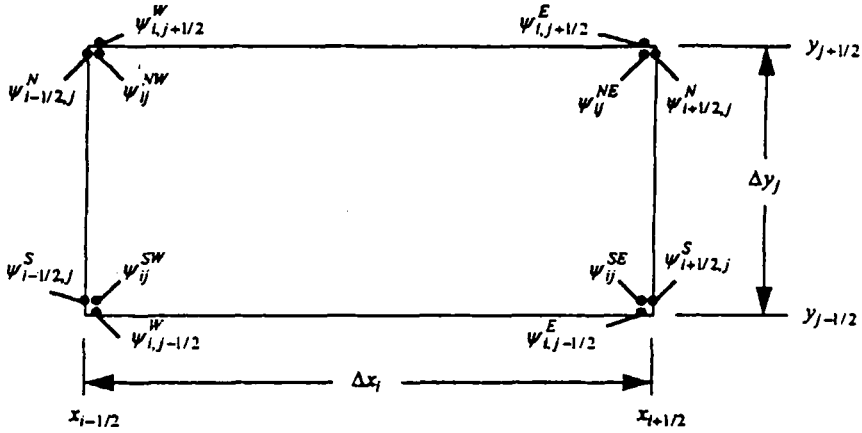
Figure 2. Notation used in BLD equations.

discretized streaming term,[5] the equation becomes

$$\frac{\psi_{m,ij}^{SW}+\psi_{m,ij}^{SE}}{2}-\psi_{m,i-1/2,j}^{S}+\frac{\psi_{m,ij}^{SW}+\psi_{m,ij}^{NW}}{2}-\psi_{m,i,j-1/2}^{W}+\frac{(\sigma_t \Delta x \Delta y)_{ij}}{4}\psi_{m,ij}^{SW}$$

$$=(\Delta x \Delta y)_{ij}\frac{1}{4}\left(\frac{1}{4\pi}[\sigma_t - \sigma_r]\phi + S\right)_{ij}^{SW}. \tag{16}$$

This equation corresponds to "fully lumped" BLD in the terminology of Wareing et al.,[15] who found that this "full lumping" is required to make BLD behave robustly in thick diffusive problems. If we interpret the unknowns as *averages* instead of point values, as shown in Figure 3, then Eq. (16) is exactly the SCB equation for the southwest corner of cell *ij*. [Actually, in SCB the corner-average values also serve as point values – see the closure Eqs. (12a).] That is, the SCB equations are identical to "fully lumped" BLD equations on rectangles in XY geometry. It is also easy to show that SCB is identical to LLD in slab geometry. Thus, in Cartesian geometries with simple cell shapes, when we force discontinuous finite-element methods to behave robustly in thick diffusive problems, we basically convert them into corner-balance methods.

## C. Asymptotic Analysis

Verifying that SCB is a sound method for thick diffusive problems requires analysis and testing. In this section we perform an asymptotic analysis that will
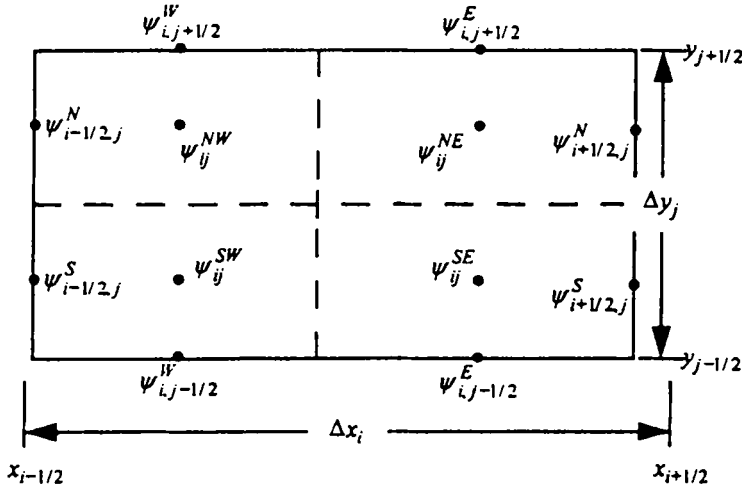
Figure 3. SCB geometric interpretation of unknowns in "fully lumped" BLD eqs.

reveal key properties of the SCB solution in such problems. This is basically the same analysis that we reviewed for the un-discretized equations in a previous section. We begin with scaled versions of the SCB equations. [See Eqs. (6), (11), and (12).]

$$\bar{\Omega}_m \cdot \left[ \bar{A}_{c+} \psi_{m,c+} + \bar{A}_{c-} \psi_{m,c-} + \bar{B}_{c+} \psi_{m,c+1/2} + \bar{B}_{c-} \psi_{m,c-1/2} \right] + \frac{\sigma_{t,c}}{\varepsilon} V_c \psi_{m,c}$$
$$= V_c \left( \frac{1}{4\pi} \left[ \frac{\sigma_{t,c}}{\varepsilon} - \varepsilon \sigma_{rc} \right] \phi_c + \varepsilon S_c \right), \tag{17}$$

$$\psi_{m,c\pm} = \begin{cases} \psi_{m,c}, & \bar{A}_{c\pm} \cdot \bar{\Omega}_m > 0, \\ \psi_{m,c\pm}^{inc}, & \bar{A}_{c\pm} \cdot \bar{\Omega}_m < 0, \end{cases} \tag{18a}$$

$$\psi_{m,c\pm1/2} = \frac{1}{2} \left( \psi_{m,c} + \psi_{m,c\pm1} \right). \tag{18b}$$

As before, we make the informed guess that the solution for small $\varepsilon$ is a power series in $\varepsilon$:

$$\psi_{m,c} = \psi_{m,c}^{(0)} + \varepsilon \psi_{m,c}^{(1)} + \varepsilon^2 \psi_{m,c}^{(2)} + \cdots \tag{19}$$

Everything now follows from the scaled equations (17) & (18) and our asymptotic ansatz (19); we simply have to perform some algebra and interpret the

results. We begin with the $O(\varepsilon^{-1})$ terms in Eq. (17), which tell us that the leading-order corner-average intensities are *isotropic:*

$$\psi_{m,c}^{(0)} = \frac{1}{4\pi}\phi_c^{(0)},\tag{20}$$

where as yet we know nothing about the leading-order scalar values $\{\phi_c^{(0)}\}$. It follows from Eq. (18b) that corner-surface unknowns in cell *interiors* are also isotropic to leading order:

$$\psi_{m,c\pm 1/2}^{(0)} = \frac{1}{4\pi}\left(\frac{\phi_c^{(0)} + \phi_{c\pm 1}^{(0)}}{2}\right).\tag{21}$$

Leading-order unknowns on cell boundaries are *half-range* isotropic, except on the problem boundary where the incident intensity comes into play:

$$\psi_{m,c+}^{(0)} = \begin{cases} \dfrac{1}{4\pi}\phi_c^{(0)}, & \vec{A}_{c+}\cdot\vec{\Omega}_m > 0, \\[2mm] \dfrac{1}{4\pi}\phi_{k+}^{(0)}, & \vec{A}_{c+}\cdot\vec{\Omega}_m < 0. \text{ edge "}c+\text{"} \notin \text{problem boundary}, \\[2mm] \psi_{m,c+}^{inc}, & \vec{A}_{c+}\cdot\vec{\Omega}_m < 0, \text{ edge "}c+\text{"} \in \text{problem boundary}, \end{cases}\tag{22a}$$

$$\psi_{m,c-}^{(0)} = \begin{cases} \dfrac{1}{4\pi}\phi_c^{(0)}, & \vec{A}_{c-}\cdot\vec{\Omega}_m > 0, \\[2mm] \dfrac{1}{4\pi}\phi_{k-}^{(0)}, & \vec{A}_{c-}\cdot\vec{\Omega}_m < 0. \text{ edge "}c-\text{"} \notin \text{problem boundary}, \\[2mm] \psi_{m,c-}^{inc}, & \vec{A}_{c-}\cdot\vec{\Omega}_m < 0. \text{ edge "}c-\text{"} \in \text{problem boundary}, \end{cases}\tag{22b}$$

where $k\pm$ is the index of the corner that shares edge $c\pm$ with corner $c$.

The $O(1)$ terms in Eq. (17) can be integrated over all directions to give:

$$\vec{A}_{c+}\cdot\sum_{m=1}^{M} w_m\vec{\Omega}_m\psi_{m,c+}^{(0)} + \vec{A}_{c-}\cdot\sum_{m=1}^{M} w_m\vec{\Omega}_m\psi_{m,c-}^{(0)}$$

$$+\vec{B}_{c+}\cdot\sum_{m=1}^{M} w_m\vec{\Omega}_m\psi_{m,c+1/2}^{(0)} + \vec{B}_{c-}\cdot\sum_{m=1}^{M} w_m\vec{\Omega}_m\psi_{m,c-1/2}^{(0)} +\sigma_{t,c}V_c\phi_c^{(1)} = \sigma_{t,c}V_c\phi_c^{(1)}.\tag{23}$$

The last two terms cancel, and if the quadrature set properly integrates linear functions of $\vec{\Omega}$, the $c\pm 1/2$ terms vanish as well because $\psi_{m,c\pm 1/2}^{(0)}$ is isotropic. We shall assume henceforth that the quadrature set *does* properly integrate linear functions of $\vec{\Omega}$; thus Eq. (23) becomes:

$$\vec{A}_{c+} \bullet \sum_{m=1}^{M} w_m \, \vec{\Omega}_m \, \psi_{m,c+}^{(0)} + \vec{A}_{c-} \bullet \sum_{m=1}^{M} w_m \, \vec{\Omega}_m \, \psi_{m,c-}^{(0)} = 0 \, ,$$

or, if corner $c$'s vertex is in the problem interior,

$$\sum_{\vec{A}_{c+} \bullet \vec{\Omega}_m > 0} w_m \, \vec{A}_{c+} \bullet \vec{\Omega}_m \, \frac{1}{4\pi} \phi_c^{(0)} + \sum_{\vec{A}_{c+} \bullet \vec{\Omega}_m < 0} w_m \, \vec{A}_{c+} \bullet \vec{\Omega}_m \, \frac{1}{4\pi} \phi_{k+}^{(0)}$$

$$+ \sum_{\vec{A}_{c-} \bullet \vec{\Omega}_m > 0} w_m \, \vec{A}_{c-} \bullet \vec{\Omega}_m \, \frac{1}{4\pi} \phi_c^{(0)} + \sum_{\vec{A}_{c-} \bullet \vec{\Omega}_m < 0} w_m \, \vec{A}_{c-} \bullet \vec{\Omega}_m \, \frac{1}{4\pi} \phi_{k-}^{(0)} = 0 \, ,$$

where $k\pm$ is the index of the corner bordering on corner $c$ at edge $c\pm$. Then:

$$\left( \phi_c^{(0)} - \phi_{k+}^{(0)} \right) \sum_{\vec{A}_{c+} \bullet \vec{\Omega}_m > 0} w_m \, \vec{A}_{c+} \bullet \vec{\Omega}_m - \left( \phi_{k-}^{(0)} - \phi_c^{(0)} \right) \sum_{\vec{A}_{c-} \bullet \vec{\Omega}_m > 0} w_m \, \vec{A}_{c-} \bullet \vec{\Omega}_m = 0 \, . \tag{24}$$

It follows from this equation (after some manipulation) that *the leading-order corner-averaged $\phi$'s around an interior vertex are equal.* That is, if corner $c$'s vertex is not on the problem boundary, then

$$\phi_{k-}^{(0)} = \phi_c^{(0)} = \phi_{k+}^{(0)} = \cdots \tag{25}$$

In other words, the leading-order corner-averaged intensities are continuous at interior vertices.

Having discovered continuity in the interior, we turn to the boundary. Suppose that edge $c+$ is on the problem boundary. Then Eq. (24) still holds provided we define

$$\phi_{k+}^{(0)} = \frac{1}{\rho_{c+}} 4 \sum_{\vec{n}_{c+} \bullet \vec{\Omega}_m < 0} w_m \left| \vec{n}_{c+} \bullet \vec{\Omega}_m \right| \psi_{m,c+}^{inc} \, , \quad \text{edge ``}c+\text{''} \in \text{problem boundary,} \tag{26a}$$

where

$$\rho_{c\pm} = \frac{1}{\pi} \sum_{\vec{n}_{c\pm} \bullet \vec{\Omega}_m < 0} w_m \left| \vec{n}_{c\pm} \bullet \vec{\Omega}_m \right| \approx 1 \, , \tag{26b}$$

$$\vec{n}_{c\pm} = \vec{A}_{c\pm} / \left| \vec{A}_{c\pm} \right| \, . \tag{26c}$$

A similar result holds for $\phi_{k-}^{(0)}$ if edge $c-$ is on the boundary. We remark that the quantities we have defined on boundary edges are "Marshak" quantities: cosine-weighted integrals of incident intensities.

Equation (17)'s $O(\varepsilon)$ terms can now be integrated over all directions to yield

$$\vec{A}_{c+} \bullet \vec{J}_{c+}^{(1)} + \vec{A}_{c-} \bullet \vec{J}_{c-}^{(1)} + \vec{B}_{c+} \bullet \vec{J}_{c+1/2}^{(1)} + \vec{B}_{c-} \bullet \vec{J}_{c-1/2}^{(1)} + \sigma_{r,c} V_c \phi_c^{(0)} = V_c S_{0,c} \, , \tag{27}$$

where we have defined order-$\varepsilon$ *net fluxes* or *net current densities:*

$$\bar{J}_{c\pm}^{(1)} = \sum_{m=1}^{M} w_m \, \bar{\Omega}_m \psi_{m,c\pm}^{(1)}, \qquad \bar{J}_{c\pm1/2}^{(1)} = \sum_{m=1}^{M} w_m \, \bar{\Omega}_m \psi_{m,c\pm1/2}^{(1)} \ . \tag{28}$$

Equation (27) is a statement of photon energy balance (or conservation) for corner $c$. If we sum such balance equations for all the corners that touch a given interior vertex, we obtain a balance equation for a *dual cell* around that vertex:

$$\sum_{c@p} \left( \bar{B}_{c+} \cdot \bar{J}_{c+1/2}^{(1)} + \bar{B}_{c-} \cdot \bar{J}_{c-1/2}^{(1)} \right) + \sum_{c@p} \sigma_{r,c} V_c \phi_c^{(0)} = \sum_{c@p} V_c S_{0,c} \ .$$

See Figure 4 for a description of this dual cell. We recognize that all the corner $\phi^{(0)}$'s in this equation are equal [see Eq. (25)], and we define a "point" notation, $\phi_p^{(0)}$, to represent them. Then our dual-cell balance equation becomes

$$\sum_{c@p} \left( \bar{B}_{c+} \cdot \bar{J}_{c+1/2}^{(1)} + \bar{B}_{c-} \cdot \bar{J}_{c-1/2}^{(1)} \right) + \phi_p^{(0)} \sum_{c@p} \sigma_{r,c} V_c = \sum_{c@p} V_c S_{0,c} \ . \tag{29}$$

Of course, the balance equation (29) does not by itself describe the behavior of SCB in thick diffusive problems — it must be supplemented by equations that relate the net fluxes on dual-cell surfaces $\left( \bar{J}_{c\pm1/2}^{(1)} \right)$ to the integrated intensities at the points $\left( \phi_p^{(0)} \right)$. To find these relations we turn first to the $O(\varepsilon)$ terms in Eq. (18b) to find:

$$\psi_{m,c\pm1/2}^{(1)} = \frac{1}{2} \left( \psi_{m,c}^{(1)} + \psi_{m,c\pm1}^{(1)} \right),$$

which means

$$\bar{J}_{c\pm1/2}^{(1)} = \frac{1}{2} \left( \bar{J}_c^{(1)} + \bar{J}_{c\pm1}^{(1)} \right). \tag{30}$$

Thus, to obtain expressions for the dual-cell-surface net fluxes, we must first find expressions for corner-average net fluxes. We obtain these by multiplying Eq. (17) by $\bar{\Omega}_m$ and integrating the $O(1)$ terms over all directions:

$$\bar{A}_{c+} \cdot \sum_{m=1}^{M} w_m \, \bar{\Omega}_m \bar{\Omega}_m \psi_{m,c+}^{(0)} + \bar{A}_{c-} \cdot \sum_{m=1}^{M} w_m \, \bar{\Omega}_m \bar{\Omega}_m \psi_{m,c-}^{(0)} + \bar{B}_{c+} \cdot \sum_{m=1}^{M} w_m \, \bar{\Omega}_m \bar{\Omega}_m \psi_{m,c+1/2}^{(0)}$$

$$+ \bar{B}_{c-} \cdot \sum_{m=1}^{M} w_m \, \bar{\Omega}_m \bar{\Omega}_m \psi_{m,c-1/2}^{(0)} + \sigma_{t,c} V_c \bar{J}_c^{(1)} = 0. \tag{31}$$

If corner $c$ is in the problem interior (not on the boundary), then each corner-surface angular intensity in this equation is isotropic, as we saw from Eqs. (21),
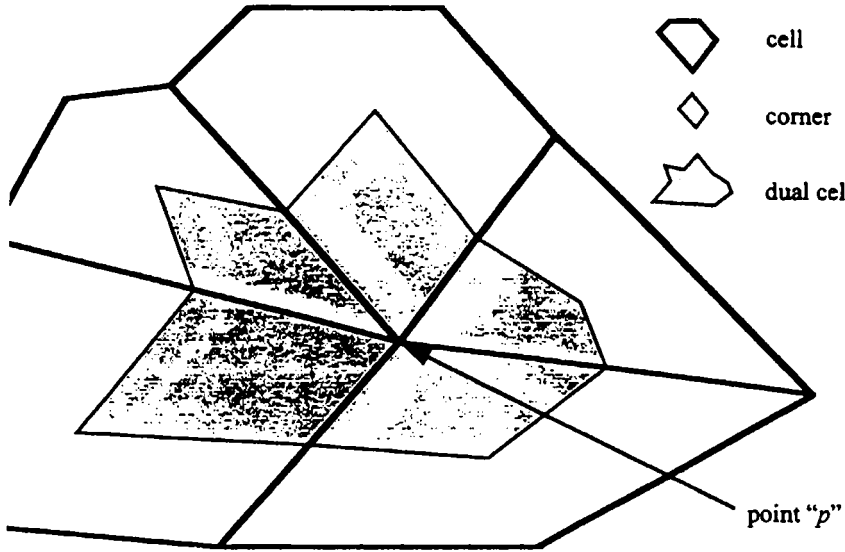
Figure 4. A dual cell, which is the union of corners about a point.

(22), and (25). If we assume (and we shall) that our quadrature set properly integrates quadratic functions of $\bar{\Omega}_m$, then we have

$$\frac{1}{3}\left[ \bar{A}_{c+}\phi_c^{(0)} + \bar{A}_{c-}\phi_c^{(0)} + \bar{B}_{c+}\frac{\phi_c^{(0)} + \phi_{c+1}^{(0)}}{2} + \bar{B}_{c-}\frac{\phi_c^{(0)} + \phi_{c-1}^{(0)}}{2} \right]$$
$$+ \sigma_{t,c}V_c\bar{J}_c^{(1)} = 0, \quad c \notin \text{boundary}. \tag{32}$$

(We shall address boundary corners later.) It follows that

$$\bar{B}_{c+} \cdot \bar{J}_{c+1/2}^{(1)} = -\frac{\bar{B}_{c+} \cdot}{6\sigma_{t,c}V_c}\left[ \bar{A}_{c+}\phi_c^{(0)} + \bar{A}_{c-}\phi_c^{(0)} + \bar{B}_{c+}\frac{\phi_c^{(0)} + \phi_{c+1}^{(0)}}{2} + \bar{B}_{c-}\frac{\phi_c^{(0)} + \phi_{c-1}^{(0)}}{2} \right]$$
$$-\frac{\bar{B}_{c+} \cdot}{6\sigma_{t,c+1}V_{c+1}}\left[ \bar{A}_{c+1,-}\phi_{c+1}^{(0)} + \bar{A}_{c+1,+}\phi_{c+1}^{(0)} - \bar{B}_{c+}\frac{\phi_c^{(0)} + \phi_{c+1}^{(0)}}{2} + \bar{B}_{c+1,+}\frac{\phi_{c+1}^{(0)} + \phi_{c+2}^{(0)}}{2} \right], \tag{33}$$
$$c, c+1 \notin \text{boundary}.$$

Let us summarize what we have found thus far. The leading-order SCB intensities in a thick diffusive region are isotropic [Eq. (21)]. The corner-average energy densities are equal, to leading order, in all corners about a given interior

vertex [Eq. (25)]. These energy densities satisfy a conservation equation over a dual cell that is the union of corner volumes about the vertex [Eq. (29)]. The net fluxes on the surfaces of the dual cell are given in terms of the leading-order energy densities by Eq. (33). Thus, if we consider Eq. (33) to be a reasonable discretization of the exact equation $\vec{J}^{(1)} = -(1/3\sigma)\vec{\nabla}\phi^{(0)}$, we conclude that the leading-order SCB solution in the interior of a thick diffusive region satisfies a reasonable discretization of the correct diffusion equation. In the next subsection we investigate how good this discretization is. First, however, we must address what happens at problem boundaries.

Discrete equations satisfied by leading-order interior solutions are not the entire story in thick diffusive problems. There is also the question of what boundary conditions a given method's interior solution satisfies. To address this for SCB, suppose corner $c$ is on the problem boundary but corner $c+1$ is interior. Then Eq. (31) tells us:

$$\sum_{\vec{A}_{c-}\cdot\vec{\Omega}_m<0} w_m\, \vec{A}_{c-}\cdot\vec{\Omega}_m\vec{\Omega}_m\psi^{(0)}_{m,c-} + \sum_{\vec{A}_{c-}\cdot\vec{\Omega}_m>0} w_m\, \vec{A}_{c-}\cdot\vec{\Omega}_m\vec{\Omega}_m\frac{\phi^{(0)}_c}{4\pi}$$

$$+\frac{1}{3}\left[\vec{A}_{c+}\phi_c^{(0)} + \vec{B}_{c+}\frac{\phi_c^{(0)}+\phi_{c+1}^{(0)}}{2} + \vec{B}_{c-}\frac{\phi_c^{(0)}+\phi_{c-1}^{(0)}}{2}\right] + \sigma_{t,c}V_c\vec{J}_c^{(1)} = 0. \tag{34}$$

We separate the incident direction into its normal and tangential components:

$$\vec{\Omega}_m = \left(\vec{n}_{c-}\cdot\vec{\Omega}_m\right)\vec{n}_{c-} + \vec{\omega}_m, \quad \text{where} \quad \vec{\omega}_m \equiv \vec{\Omega}_m - \left(\vec{n}_{c-}\cdot\vec{\Omega}_m\right)\vec{n}_{c-} \quad \text{and}$$

$$\vec{n}_{c-} \equiv \vec{A}_{c-}\big/\left|\vec{A}_{c-}\right|. \tag{35}$$

Then

$$\sum_{\vec{A}_{c-}\cdot\vec{\Omega}_m<0} w_m\, \vec{A}_{c-}\cdot\vec{\Omega}_m\vec{\Omega}_m\psi^{inc}_{m,c-} + \sum_{\vec{A}_{c-}\cdot\vec{\Omega}_m>0} w_m\, \vec{A}_{c-}\cdot\vec{\Omega}_m\vec{\Omega}_m\frac{\phi^{(0)}_c}{4\pi}$$

$$=\left|\vec{A}_{c-}\right|\sum_{\vec{A}_{c-}\cdot\vec{\Omega}_m<0} w_m\,\vec{n}_{c-}\cdot\vec{\Omega}_m\left[\left(\vec{n}_{c-}\cdot\vec{\Omega}_m\right)\vec{n}_{c-} + \vec{\omega}_m\right]\psi^{inc}_{m,c-} + \frac{1}{6}\vec{A}_{c-}\phi_c^{(0)}$$

$$=\vec{A}_{c-}\sum_{\vec{A}_{c-}\cdot\vec{\Omega}_m<0} w_m\left(\vec{n}_{c-}\cdot\vec{\Omega}_m\right)^2\psi^{inc}_{m,c-} + \frac{1}{6}\vec{A}_{c-}\phi_c^{(0)} + \sum_{\vec{A}_{c-}\cdot\vec{\Omega}_m<0} w_m\, \vec{A}_{c-}\cdot\vec{\Omega}_m\vec{\omega}_m\psi^{inc}_{m,c-}. \tag{36}$$

Before we can understand what this means we must determine $\phi_c^{(0)}$ as a function of incident intensities. Referring to Figure 5 and considering the $N$ corners that
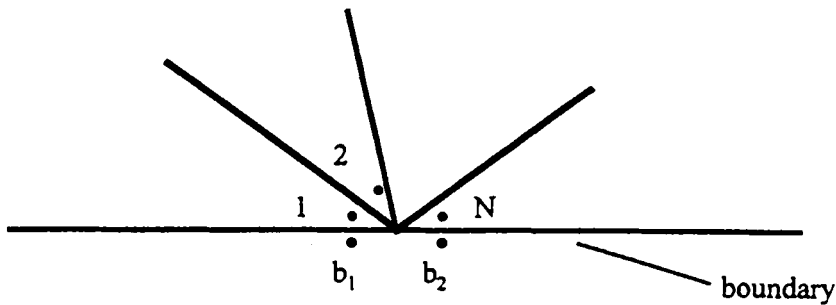
Figure 5. Numbering used in Eq. (37).

touch a given boundary point, we see that Eqs. (24) are of the form:

$$
\begin{bmatrix}
a_1+a_2 & -a_2 & 0 & \cdots & & 0 \\
-a_2 & a_2+a_3 & -a_3 & \ddots & & \vdots \\
0 & -a_3 & \ddots & & & 0 \\
\vdots & & \ddots & \ddots & & -a_N \\
0 & \cdots & & 0 & -a_N & a_N+a_{N+1}
\end{bmatrix}
\begin{bmatrix}
\phi_1^{(0)} \\
\phi_2(0) \\
\vdots \\
\phi_{N-1}^{(0)} \\
\phi_N^{(0)}
\end{bmatrix}
=
\begin{bmatrix}
a_1\phi_{b1} \\
0 \\
\vdots \\
0 \\
a_{N+1}\phi_{b2}
\end{bmatrix},
\qquad (37)
$$

where, each $a_i$ is positive, and where, for example,

$$
a_1 = \sum_{\vec{A}_1-\cdot\vec{\Omega}_m>0} w_m \, \vec{A}_{1-}\cdot\vec{\Omega}_m, \tag{38a}
$$

$$
a_2 = \sum_{\vec{A}_{1+}\cdot\vec{\Omega}_m>0} w_m \, \vec{A}_{1+}\cdot\vec{\Omega}_m = \sum_{\vec{A}_2-\cdot\vec{\Omega}_m>0} w_m \, \vec{A}_{2-}\cdot\vec{\Omega}_m, \tag{38b}
$$

$$
\phi_{b1} = 2 \sum_{\vec{n}_1-\cdot\vec{\Omega}_m<0} w_m 2 \frac{|\vec{n}_1-\cdot\vec{\Omega}_m|}{\rho_{b1}} \psi_{m,b1}^{inc}, \qquad \rho_{b1} = \frac{\displaystyle\sum_{\vec{n}_1-\cdot\vec{\Omega}_m<0} w_m |\vec{n}_1-\cdot\vec{\Omega}_m|}{\pi} \approx 1. \tag{38c}
$$

The matrix in Eq. (37) is a symmetric positive-definite "M-matrix," whose inverse is symmetric and has strictly non-negative entries. This means each unknown on the left-hand side is a linear combination of $\phi_{b1}$ and $\phi_{b2}$, which are "Marshak-boundary" energy densities. Thus, if corner $c$ touches a boundary point, *the corner-averaged energy density, $\phi_c^{(0)}$, is a weighted average of the two Marshak energy densities that are incident at that boundary point.* This is the

same as a cosine-weighted integral of an *incident intensity that is a weighted average of the two incident intensities* on either side of the boundary point.

Focusing once again on Eq. (36), in which the $A_{c-}$ surface is on a boundary, and replacing $\phi_c^{(0)}$ by a cosine-weighted integral of a weighted-average incident intensity, we now have

$$
\sum_{\bar{A}_{c-}\cdot\bar{\Omega}_m<0} w_m\,\bar{A}_{c-}\cdot\bar{\Omega}_m\bar{\Omega}_m\,\psi_{m,c-}^{inc} + \sum_{\bar{A}_{c-}\cdot\bar{\Omega}_m>0} w_m\,\bar{A}_{c-}\cdot\bar{\Omega}_m\bar{\Omega}_m\,\frac{\phi_c^{(0)}}{4\pi}
$$

$$
= \frac{1}{3}\bar{A}_{c-}\sum_{\bar{n}_{c-}\cdot\bar{\Omega}_m<0} w_m\,3\big(\bar{n}_{c-}\cdot\bar{\Omega}_m\big)^2\psi_{m,c-}^{inc} + \frac{1}{3}\bar{A}_{c-}\sum_{\bar{n}_{c-}\cdot\bar{\Omega}_m<0} w_m\,2\frac{|\bar{n}_{c-}\cdot\bar{\Omega}_m|}{\rho_{c-}}\Big\langle\psi_{m,c-}^{inc}\Big\rangle
$$

$$
+ \sum_{\bar{n}_{c-}\cdot\bar{\Omega}_m<0} w_m\,\bar{A}_{c-}\cdot\bar{\Omega}_m\bar{\omega}_m\,\psi_{m,c-}^{inc}
$$

$$
= \frac{1}{3}\bar{A}_{c-}\sum_{\bar{n}_{c-}\cdot\bar{\Omega}_m<0} w_m\left[2\frac{|\bar{n}_{c-}\cdot\bar{\Omega}_m|}{\rho_{c-}}\Big\langle\psi_{m,c-}^{inc}\Big\rangle + 3\big(\bar{n}_{c-}\cdot\bar{\Omega}_m\big)^2\psi_{m,c-}^{inc}\right]
$$

$$
+ \sum_{\bar{n}_{c-}\cdot\bar{\Omega}_m<0} w_m\,\bar{A}_{c-}\cdot\bar{\Omega}_m\bar{\omega}_m\,\psi_{m,c-}^{inc} \,, \tag{39}
$$

where $\big\langle\psi_{m,c-}^{inc}\big\rangle$ is a weighted average of the two incident intensities on either side of the boundary point at corner $c$. The first term on the right-hand side of Eq. (39) will function in Eq. (34) as a Dirichlét boundary condition on the boundary vertex associated with corner $c$. This leads us to define the "boundary-condition" energy density:

$$
\phi_{c-}^{b.c.} = \sum_{\bar{n}_{c-}\cdot\bar{\Omega}_m<0} w_m\left[2\frac{|\bar{n}_{c-}\cdot\bar{\Omega}_m|}{\rho_{c-}}\Big\langle\psi_{m,c-}^{inc}\Big\rangle + 3\big(\bar{n}_{c-}\cdot\bar{\Omega}_m\big)^2\psi_{m,c-}^{inc}\right]. \tag{40}
$$

Note that this is a reasonable facsimile of the boundary condition satisfied by the exact leading-order interior solution [recall Eqs. (9) and (10)]:

$$
\phi_{exact}^{(0)}(\bar{r}_s) = \int_{\bar{n}\cdot\bar{\Omega}<0} d\Omega\,\sqrt{3}\,|\bar{n}\cdot\bar{\Omega}|\,H\big(|\bar{n}\cdot\bar{\Omega}|\big)\psi_{inc}(\bar{r}_s,\bar{\Omega})
$$

$$
\approx \int_{\bar{n}\cdot\bar{\Omega}<0} d\Omega\left[2|\bar{n}\cdot\bar{\Omega}| + 3\big(\bar{n}\cdot\bar{\Omega}\big)^2\right]\psi_{inc}(\bar{r}_s,\bar{\Omega}). \tag{41}
$$

We can now rewrite Eq. (34), for the case of corner $c$ on the boundary but $c+1$ interior, as follows:

$$\sum_{\bar{n}_{c-} \cdot \vec{\Omega}_m < 0} w_m \, \bar{A}_{c-} \cdot \vec{\Omega}_m \bar{\omega}_m \psi_{m,c-}^{inc}$$

$$+ \frac{1}{3} \left[ \bar{A}_{c+} \phi_c^{(0)} + \bar{A}_{c-} \phi_{c-}^{b.c.} + \bar{B}_{c+} \frac{\phi_c^{(0)} + \phi_{c+1}^{(0)}}{2} + \bar{B}_{c-} \frac{\phi_c^{(0)} + \phi_{c-1}^{(0)}}{2} \right] + \sigma_{t,c} V_c \bar{J}_c^{(1)} = 0. \tag{42}$$

It is convenient to define:

$$F_{c-} = \begin{cases} \phi_c^{(0)}, & c- \notin \text{boundary,} \\[2mm] \displaystyle\sum_{\bar{n}_{c-} \cdot \vec{\Omega}_m < 0} w_m \left[ 2 \frac{|\bar{n}_{c-} \cdot \vec{\Omega}_m|}{\rho_{c-}} \left\langle \psi_{m,c-}^{inc} \right\rangle + 3 \left(\bar{n}_{c-} \cdot \vec{\Omega}_m\right)^2 \psi_{m,c-}^{inc} \right], & c- \in \text{boundary,} \end{cases} \tag{43a}$$

$$F_{c+} = \begin{cases} \phi_c^{(0)}, & c+ \notin \text{boundary,} \\[2mm] \displaystyle\sum_{\bar{n}_{c+} \cdot \vec{\Omega}_m < 0} w_m \left[ 2 \frac{|\bar{n}_{c+} \cdot \vec{\Omega}_m|}{\rho_{c+}} \left\langle \psi_{m,c+}^{inc} \right\rangle + 3 \left(\bar{n}_{c+} \cdot \vec{\Omega}_m\right)^2 \psi_{m,c+}^{inc} \right], & c+ \in \text{boundary.} \end{cases} \tag{43b}$$

We also shall need to define some rather odd-looking terms that, as we shall see later, can sometimes have the effect of artificial sources. For a corner $c$ that touches an interior vertex, with corners $c+1$ and/or $c-1$ possibly touching boundaries, we define:

$$V_c \widetilde{S}_{c+1/2} = \begin{cases} 0, & (c+1,+) \notin \text{boundary,} \\[2mm] \displaystyle\frac{1}{2(\sigma_t V)_{c+1}} \sum_{\bar{n}_{c+1,+} \cdot \vec{\Omega}_m < 0} w_m \left( \bar{A}_{c+1,+} \cdot \vec{\Omega}_m \right)\left( \bar{B}_{c+} \cdot \bar{\omega}_m \right) \psi_{m,c+1,+}^{inc}, & (c+1,+) \in \text{bdy,} \end{cases} \tag{44a}$$

$$V_c \widetilde{S}_{c-1/2} = \begin{cases} 0, & (c-1,-) \notin \text{boundary,} \\[2mm] \displaystyle\frac{1}{2(\sigma_t V)_{c-1}} \sum_{\bar{n}_{c-1,-} \cdot \vec{\Omega}_m < 0} w_m \left( \bar{A}_{c-1,-} \cdot \vec{\Omega}_m \right)\left( \bar{B}_{c-} \cdot \bar{\omega}_m \right) \psi_{m,c-1,-}^{inc}, & (c-1,-) \in \text{bdy.} \end{cases} \tag{44b}$$

After combining Eqs. (30), (42), (43), and (44), we finally obtain a general expression for the next flux across each surface of a dual cell about the interior point $p$. If corner $c$ touches the interior point $p$, then this general expression takes the form:

$$\bar{B}_{c+} \cdot \bar{J}_{c+1/2}^{(1)} = -V_c \widetilde{S}_{c+1/2} - \frac{\bar{B}_{c+} \cdot}{6\sigma_{t,c} V_c} \left[ \bar{A}_{c+} \phi_c^{(0)} + \bar{A}_{c-} \phi_c^{(0)} + \bar{B}_{c+} \frac{\phi_c^{(0)} + \phi_{c+1}^{(0)}}{2} + \bar{B}_{c-} \frac{\phi_c^{(0)} + \phi_{c-1}^{(0)}}{2} \right]$$

$$- \frac{\bar{B}_{c+} \cdot}{6\sigma_{t,c+1} V_{c+1}} \left[ \bar{A}_{c+1,-} F_{c+1,-} + \bar{A}_{c+1,+} F_{c+1,+} - \bar{B}_{c+} \frac{\phi_c^{(0)} + \phi_{c+1}^{(0)}}{2} + \bar{B}_{c+1,+} \frac{\phi_{c+1}^{(0)} + \phi_{c+2}^{(0)}}{2} \right]. \tag{45}$$

The differences between this and Eq. (33) are: 1) the $(2\mu+3\mu^2)$-weighted energy

densities $F_{c+1,\pm}$ are used on boundary surfaces, and  2) there is an "artificial source" term present. In the next subsection we shall explore what this all means.

### D.  Interpretation of Analysis

Rectangular grids offer the simplest setting in which to interpret the analysis performed above.  Given such a grid and the notation of Figure 2, we have from Eq. (25):

$$\phi_{i+1/2,j+1/2} = \phi_{ij}^{NE(0)} = \phi_{i+1,j}^{NW(0)} = \phi_{i+1,j+1}^{SW(0)} = \phi_{i,j+1}^{SE(0)}, \quad i=1,...,I-1, \quad j=1,...,K-1, \quad (46)$$

where $I$ and $K$ are the number of cells in the $x$ and $y$ directions, respectively.  This is a statement of continuity and the definition of a convenient notation to describe the continuous quantity at each interior vertex.  Equation (29) on a rectangular grid becomes:

$$\frac{\Delta y_{j+1}}{2}\left[J_{x,i+1,j+1}^{S(1)} - J_{x,i,j+1}^{S(1)}\right] + \frac{\Delta y_j}{2}\left[J_{x,i+1,j}^{N(1)} - J_{x,i,j}^{N(1)}\right]$$

$$+ \frac{\Delta x_{i+1}}{2}\left[J_{y,i+1,j+1}^{W(1)} - J_{y,i+1,j}^{W(1)}\right] + \frac{\Delta x_i}{2}\left[J_{y,i,j+1}^{E(1)} - J_{y,i,j}^{E(1)}\right]$$

$$+ \left[\frac{(\sigma_r \Delta x \Delta y)_{i+1,j+1} + (\sigma_r \Delta x \Delta y)_{i+1,j} + (\sigma_r \Delta x \Delta y)_{i,j+1} + (\sigma_r \Delta x \Delta y)_{ij}}{4}\right]\phi_{i+1/2,j+1/2}$$

$$= \frac{\left(\Delta x \Delta y S_0^{SW}\right)_{i+1,j+1} + \left(\Delta x \Delta y S_0^{NW}\right)_{i+1,j} + \left(\Delta x \Delta y S_0^{SE}\right)_{i,j+1} + \left(\Delta x \Delta y S_0^{NE}\right)_{ij}}{4}. \quad (47)$$

This is simply a statement of conservation over the "dual-cell" rectangle that goes from $(x_i, y_j)$ to $(x_{i+1}, y_{j+1})$.  Equation (45) gives us the net fluxes $J$ in terms of the energy densities; on a rectangular grid this is, for example,

$$\frac{\Delta y_j}{2}J_{x,i+1,j}^{N(1)} = -\frac{\Delta y_j}{2}\frac{F_{i+3/2,j}^N - F_{i+1/2,j}^N}{3\sigma_{i+1,j}\Delta x_{i+1}}, \quad (48)$$

where

$$F_{i+1/2,j}^N = \begin{cases} \phi_{i+1/2,j+1/2}^{(0)}, & i \neq 0, \\ \sum_{\mu_m>0} w_m\left[2\frac{|\mu_m|}{\rho}\left\langle \psi_{m,1/2,j}^{inc,N}\right\rangle + 3\mu_m^2 \psi_{m,1/2,j}^{inc,N}\right], & i = 0, \end{cases} \quad (49a)$$

$$F_{i+3/2,j}^N = \begin{cases} \phi_{i+3/2,j+1/2}^{(0)}, & i \neq I-1, \\ \sum_{\mu_m<0} w_m\left[2\frac{|\mu_m|}{\rho}\left\langle \psi_{m,i+1/2,j}^{inc,N}\right\rangle + 3\mu_m^2 \psi_{m,i+1/2,j}^{inc,N}\right], & i = I-1, \end{cases} \quad (49b)$$

$$\left\langle \psi_{m,1/2,J}^{inc,N} \right\rangle = \frac{\psi_{m,1/2,J}^{N}\left(1 + \Delta x_1/\Delta y_J\right) + \psi_{m,1/2,J+1}^{S}\,\Delta x_1/\Delta y_{J+1}}{1 + \Delta x_1/\Delta y_J + \Delta x_1/\Delta y_{J+1}}, \tag{50a}$$

$$\left\langle \psi_{m,I+1/2,J}^{inc,N} \right\rangle = \frac{\psi_{m,I+1/2,J}^{N}\left(1 + \Delta x_I/\Delta y_J\right) + \psi_{m,I+1/2,J+1}^{S}\,\Delta x_I/\Delta y_{J+1}}{1 + \Delta x_I/\Delta y_J + \Delta x_I/\Delta y_{J+1}}. \tag{50b}$$

Note that the "artificial source" terms and many of the dot products in Eq. (47) disappear on a rectangular grid.

The meaning of all this becomes clearer if we insert Eqs. (48) (and similar equations) into Eq. (47) and rearrange:

$$-\frac{1}{2}\left(\frac{\Delta y_{j+1}}{3\sigma_{i+1,j+1}} + \frac{\Delta y_j}{3\sigma_{i+1,j}}\right)\frac{\Phi_{i+3/2,j+1/2} - \Phi_{i+1/2,j+1/2}}{\Delta x_{i+1}} + \frac{1}{2}\left(\frac{\Delta y_{j+1}}{3\sigma_{i,j+1}} + \frac{\Delta y_j}{3\sigma_{i,j}}\right)\frac{\Phi_{i+1/2,j+1/2} - \Phi_{i-1/2,j+1/2}}{\Delta x_{i+1}}$$

$$-\frac{1}{2}\left(\frac{\Delta x_{i+1}}{3\sigma_{i+1,j+1}} + \frac{\Delta x_i}{3\sigma_{i,j+1}}\right)\frac{\Phi_{i+1/2,j+3/2} - \Phi_{i+1/2,j+1/2}}{\Delta y_{j+1}} + \frac{1}{2}\left(\frac{\Delta x_{i+1}}{3\sigma_{i+1,j}} + \frac{\Delta x_i}{3\sigma_{i,j}}\right)\frac{\Phi_{i+1/2,j+1/2} - \Phi_{i+1/2,j-1/2}}{\Delta y_j}$$

$$+\left[\frac{(\sigma_r \Delta x \Delta y)_{i+1,j+1} + (\sigma_r \Delta x \Delta y)_{i+1,j} + (\sigma_r \Delta x \Delta y)_{i,j+1} + (\sigma_r \Delta x \Delta y)_{ij}}{4}\right]\Phi_{i+1/2,j+1/2}$$

$$= \frac{\left(\Delta x \Delta y S_0^{SW}\right)_{i+1,j+1} + \left(\Delta x \Delta y S_0^{NW}\right)_{i+1,j} + \left(\Delta x \Delta y S_0^{SE}\right)_{i,j+1} + \left(\Delta x \Delta y S_0^{NE}\right)_{ij}}{4}. \tag{51}$$

Here we have defined:

$$\Phi_{i+1/2,j+1/2} \equiv \begin{cases} \phi_{i+1/2,j+1/2}, i = 1,\ldots,I-1, \quad j = 1,\ldots,K-1, \\[2mm] \dfrac{\left(\Delta y_{j+1}/\sigma_{1,j+1}\right)F_{1/2,j+1}^{S} + \left(\Delta y_j/\sigma_{1,j}\right)F_{1/2,j}^{N}}{\left(\Delta y_{j+1}/\sigma_{1,j+1}\right) + \left(\Delta y_j/\sigma_{1,j}\right)}, i = 0, \quad j = 1,\ldots,K-1, \\[3mm] \dfrac{\left(\Delta y_{j+1}/\sigma_{I,j+1}\right)F_{I+1/2,j+1}^{S} + \left(\Delta y_j/\sigma_{I,j}\right)F_{I+1/2,j}^{N}}{\left(\Delta y_{j+1}/\sigma_{I,j+1}\right) + \left(\Delta y_j/\sigma_{I,j}\right)}, i = I, j = 1,\ldots,K-1, \\[3mm] \dfrac{\left(\Delta x_{i+1}/\sigma_{i+1,1}\right)F_{i+1,1/2}^{W} + \left(\Delta x_i/\sigma_{i,1}\right)F_{i,1/2}^{E}}{\left(\Delta x_{i+1}/\sigma_{i+1,1}\right) + \left(\Delta x_i/\sigma_{i,1}\right)}, i = 1,\ldots,I-1, \quad j = 0, \\[3mm] \dfrac{\left(\Delta x_{i+1}/\sigma_{i+1,K}\right)F_{i+1,K+1/2}^{W} + \left(\Delta x_i/\sigma_{i,K}\right)F_{i,K+1/2}^{E}}{\left(\Delta x_{i+1}/\sigma_{i+1,1}\right) + \left(\Delta x_i/\sigma_{i,1}\right)}, i = 1,\ldots,I-1, j = K. \end{cases} \tag{52}$$

Equation (51) is a standard 5-point diffusion discretization for the vertex quantities $\Phi$. At interior vertices these quantities are simply the leading-order

energy densities, as we see from Eq. (45) and the first line of Eq. (52). At a boundary vertex, $\Phi$ is an excellent approximation to the analytic boundary condition given in Eqs. (9) and (10). For example, from Eqs. (49), (50), and (52), we can find:

$$\Phi_{1/2,j+1/2} = \sum_{\mu_m>0} w_m \left[ 2\frac{|\mu_m|}{\rho} \frac{\psi^{inc,S}_{m,1/2,j+1}\beta^S_{1/2,j+1/2} + \psi^{inc,N}_{m,1/2,j}\beta^N_{1/2,j+1/2}}{\beta^S_{1/2,j+1/2} + \beta^N_{1/2,j+1/2}} + 3\mu_m^2 \frac{\psi^{inc,S}_{m,1/2,j+1}\sigma_{1,j}\Delta y_{j+1} + \psi^{inc,N}_{m,1/2,j}\sigma_{1,j+1}\Delta y_j}{\sigma_{1,j}\Delta y_{j+1} + \sigma_{1,j+1}\Delta y_j} \right], \qquad (53)$$

where

$$\beta^S_{1/2,j+1/2} = \sigma_{1,j}\Delta y_j\Delta y^2_{j+1} + \sigma_{1,j}\Delta x_1\Delta y_j\Delta y_{j+1} + \sigma_{1,j+1}\Delta x_1\Delta y^2_j, \qquad (54a)$$

$$\beta^N_{1/2,j+1/2} = \sigma_{1,j+1}\Delta y^2_j\Delta y_{j+1} + \sigma_{1,j+1}\Delta x_1\Delta y_j\Delta y_{j+1} + \sigma_{1,j}\Delta x_1\Delta y^2_{j+1}. \qquad (54b)$$

That is, each boundary $\Phi$ is the sum of a $2\mu$-weighted integral and a $3\mu^2$-weighted integral, which is a very good approximation of the analytic boundary-condition energy density. Each integral is of a robust average of the two incident intensities on either side of the boundary vertex. This means that the leading-order interior SCB energy densities in the interior not only satisfy a robust 5-point diffusion discretization [Eq. (51)], but also very accurate boundary conditions [Eq. (53)]. This is the precise analog of the lumped LD method in slab geometry. This is a very strong result, and to our knowledge corner balance methods are the only multidimensional transport methods that attain it.

Sadly, this strong result holds only on rectangles. On a general grid of distorted polygonal cells, the following degradations can occur:

- Equation (33) may no longer be a very good discretization of $\vec{J}^{(1)} = -(1/3\sigma)\vec{\nabla}\phi^{(0)}$. On a rectangular grid, Eq. (33) leads ultimately to Eq. (51), which has the important property that it is exact if $\vec{\nabla}\phi^{(0)}$ is constant. In general, though, Eq. (33) can introduce error even when $\vec{\nabla}\phi^{(0)}$ is constant. The physical effect of this is that the diffusion coefficient (which should simply be $[3\sigma_i]^{-1}$) is effectively too large in some parts of the problem and too small in others. Thus, we cannot claim that on a general distorted grid the leading-order SCB solution satisfies a robust discretization of the correct diffusion equation. It does satisfy a diffusion discretization, but with an inexact diffusion coefficient if

the grid is distorted. We remark, however. that it is very difficult to create a diffusion discretization that is accurate and robust on arbitrary grids; thus, designing a transport discretization that performs well on diffusive problems with such grids is a bit like shooting at a hidden target. We will address this further in our concluding remarks at the end of this paper.

- As shown in Eq. (45), there can be an "artificial" source term, which can be positive or negative, introduced at boundaries. This happens only if incident intensities are azimuthally asymmetric about the surface normal *and* the boundary edge is not parallel to nearby dual-cell edges.

- If only two corners touch a boundary vertex, then each corner will have a surface that is part of the boundary, and only $(2\mu + 3\mu^2)$-weighted integrals of incident intensities at that vertex [defined in the second line of Eq. (43a) and of (43b)] will enter into expressions for net fluxes across dual-cell edges. However, if more than two corners meet at a boundary vertex, then all but two of them will have no surfaces on the boundary. (See Fig. 5.) This means that for those corners the first lines of Eqs. (43) will hold, and thus in some net-flux expressions the role of energy density at the boundary vertex will be filled by $\phi_c^{(0)}$. But each $\phi_c^{(0)}$ is a $4\mu$-weighted integral of incident intensities [see Eq. (38c)], which can be a poor approximation to the boundary condition satisfied by the exact leading-order energy density [which is more like a $(2\mu+3\mu^2)$-weighted integral].

The above can be summarized as follows. The SCB method presented here seems to be a step in the right direction for radiative transfer problems. Its behavior in thick diffusive problems with rectangular grids is exactly what we sought, and to our knowledge this is unmatched by any other discretization. The method is also easily defined on a grid of arbitrary polygonal cells. However, implementing the method on such a grid would require the solution of an N×N system of equations, where N is the number of corners in a given polygonal cell, for each cell during each transport sweep. From a practical point of view we would rather avoid this if possible. The following section describes an attempt to avoid N×N systems while retaining the good properties of SCB in thick diffusive problems.

## IV.    AN "UPSTREAM" CORNER-BALANCE (UCB) METHOD

### A.    Goals for UCB

Our SCB method is defined by a "balance" equation for each "corner" subcell in a problem plus simple "closure" equations that relate surface-averaged intensities to corner-averaged intensities.    In this section we explore how we might alter the closure equations to achieve the following:

- A discretization that allows transport sweeps to proceed corner by corner, instead of having all N corners coupled in an N-sided polygon;

- Better performance than SCB on cells of low and intermediate thickness;

- A leading-order solution in thick diffusive problems that is identical to the SCB solution, at least on rectangular grids.

The first item says we seek a method in which the unknowns in a given corner, for a given direction, depend only on outflow quantities from corners that are physically upstream; thus, we shall call this an "upstream corner-balance" (UCB) method.   The second item refers to the fact that SCB is not very accurate for thin or intermediate cells, even in slab geometry, and thus needs improvement.  This is documented in reference 16.

### B.    Development and Thick-Limit Analysis of UCB

Pursuing insight into how we might alter the SCB closures to create a UCB method, without destroying the good diffusion-limit properties of SCB, we now examine how each SCB closure equation affects the leading-order solution in a thick diffusive problem.   We repeat the closure equations here for convenience. First, on a corner surface that is also a *cell surface*, we have Eq. (18a):

$$\psi_{m,c\pm} = \begin{cases} \psi_{m,c}, & \bar{A}_{c\pm} \cdot \bar{\Omega}_m > 0, \\ \psi^{inc}_{m,c\pm}, & \bar{A}_{c\pm} \cdot \bar{\Omega}_m < 0. \end{cases} \qquad (55a)$$

This is a "step" or "backward-Euler" closure, which already has the "upstream" property we seek.  On a corner surface in the *interior* of a cell SCB uses Eq. (18b):

$$\psi_{m,c\pm1/2} = \frac{1}{2}\left(\psi_{m,c} + \psi_{m,c\pm1}\right). \qquad (55b)$$

This is an interpolatory closure that basically assumes, and takes advantage of, smoothness of the cell-interior solution. It is responsible for the dependence of a corner's intensity on intensities that are physically downstream.

The key diffusion-limit consequence of the step closure on cell surfaces is that leading-order corner-averaged energy densities will be the equal in all corners that touch a single interior vertex, as shown in Eqs. (24) and (25). We want our UCB method to retain this property, and the step closure is already "upstream," so our UCB scheme shall retain the closure (55a).

The first key consequence of the cell-interior closure (55b) is Eq. (21) – leading-order intensities on cell-interior corner surfaces are isotropic. Without this result, the cell-interior surface terms in Eq. (23) would not vanish, and the continuity result of Eq. (25) would not follow. The second key consequence of Eq. (55b) is Eq. (33), which describes the $O(\varepsilon)$ net flux across a cell-interior corner surface. Without a result similar to this, the SCB leading-order solution would not satisfy a five-point differencing scheme on a rectangular grid. The third key consequence of Eq. (55b) is the boundary condition for the leading-order interior solution, which for a rectangular grid is defined by Eq. (52). Without a similar result, the interior solution in a diffusive problem could satisfy a good diffusion discretization but inaccurate boundary conditions.

Our UCB method will consist of a conservation equation (11) for each corner, the cell-surface closure Eq. (55a), and a cell-interior closure to be determined. Let us consider the $c+1/2$ surface, and consider a closure of the following form:

$$
\psi_{m,c+1/2} = \begin{cases} \psi_{m,c} + \dfrac{1}{2}\left(\dfrac{Q}{\sigma_t/\varepsilon}\right)_{c+1} - \dfrac{1}{2}\left(\dfrac{Q}{\sigma_t/\varepsilon}\right)_{c} + [T]_{m,c\to c+1}, & \vec{B}_{c+}\cdot\vec{\Omega}_m > 0, \\[2ex] \psi_{m,c+1} + \dfrac{1}{2}\left(\dfrac{Q}{\sigma_t/\varepsilon}\right)_{c} - \dfrac{1}{2}\left(\dfrac{Q}{\sigma_t/\varepsilon}\right)_{c+1} + [T]_{m,c+1\to c}, & \vec{B}_{c+}\cdot\vec{\Omega}_m < 0, \end{cases} \tag{56}
$$

where we have inserted the asymptotic scaling and defined the total source:

$$
Q_c = \left(\frac{1}{4\pi}\left[\frac{\sigma_{tc}}{\varepsilon} - \varepsilon\sigma_{rc}\right]\phi_c + \varepsilon S_c\right). \tag{57}
$$

Equation (56) does not fully define the closure, of course, because we have not yet specified the "T" terms in the equations. For the moment we shall simply impose

the condition that the largest term in the asymptotic expansions of the "T" terms is the coefficient of $\varepsilon$:

$$[T]^{(0)}_{m,c\to c+1} = [T]^{(0)}_{m,c+1\to c} = 0.$$

Given this condition, we can determine the leading-order cell-interior-surface intensity produced by our proposed closure:

$$
\psi^{(0)}_{m,c+1/2} = \psi^{(0)}_{m,c} + \left[\frac{1}{2}\frac{\varepsilon}{\sigma_t}\left(\frac{1}{4\pi}\left[\frac{\sigma_t}{\varepsilon} - \varepsilon\sigma_r\right]\phi + \varepsilon S\right)\right]^{(0)}_{c+1}
$$

$$
-\left[\frac{1}{2}\frac{\varepsilon}{\sigma_t}\left(\frac{1}{4\pi}\left[\frac{\sigma_t}{\varepsilon} - \varepsilon\sigma_r\right]\phi + \varepsilon S\right)\right]^{(0)}_{c}
$$

$$
= \frac{\phi^{(0)}_c}{4\pi} + \left[\frac{1}{2}\frac{\phi^{(0)}_{c+1}}{4\pi}\right] - \left[\frac{1}{2}\frac{\phi^{(0)}_{c}}{4\pi}\right]
$$

$$
= \frac{1}{4\pi}\frac{\phi^{(0)}_c + \phi^{(0)}_{c+1}}{2}, \qquad \vec{B}_{c+}\cdot\vec{\Omega}_m > 0, \tag{58a}
$$

$$
\psi^{(0)}_{m,c+1/2} = \psi^{(0)}_{m,c+1} + \left[\frac{1}{2}\frac{\varepsilon}{\sigma_t}\left(\frac{1}{4\pi}\left[\frac{\sigma_t}{\varepsilon} - \varepsilon\sigma_r\right]\phi + \varepsilon S\right)\right]^{(0)}_{c}
$$

$$
-\left[\frac{1}{2}\frac{\varepsilon}{\sigma_t}\left(\frac{1}{4\pi}\left[\frac{\sigma_t}{\varepsilon} - \varepsilon\sigma_r\right]\phi + \varepsilon S\right)\right]^{(0)}_{c+1}
$$

$$
= \cdots = \frac{1}{4\pi}\frac{\phi^{(0)}_c + \phi^{(0)}_{c+1}}{2}, \qquad \vec{B}_{c+}\cdot\vec{\Omega}_m < 0. \tag{58b}
$$

Thus, the leading-order intensity is isotropic on a cell-interior corner surface, which is the first needed key result. In fact, this result is identical to that of SCB.

We turn next to the net flux across the $c+1/2$ surface. To leading order this is zero, because the intensity is isotropic; this matches the SCB and analytic results. The $O(\varepsilon)$ component is the important one, and it is:

$$
\vec{B}_{c+}\cdot\vec{J}^{(1)}_{c+1/2} = \sum_m w_m \vec{B}_{c+}\cdot\vec{\Omega}_m \psi^{(1)}_{m,c+1/2}
$$

$$
= \sum_{\vec{B}_{c-}\cdot\vec{\Omega}_m > 0} w_m \vec{B}_{c+}\cdot\vec{\Omega}_m\left[\psi^{(1)}_{m,c} + \frac{1}{4\pi}\frac{\phi^{(1)}_{c+1} - \phi^{(1)}_c}{2} + T^{(1)}_{m,c\to c+1}\right]
$$

$$
+ \sum_{\vec{B}_{c-}\cdot\vec{\Omega}_m < 0} w_m \vec{B}_{c+}\cdot\vec{\Omega}_m\left[\psi^{(1)}_{m,c+1} + \frac{1}{4\pi}\frac{\phi^{(1)}_c - \phi^{(1)}_{c+1}}{2} + T^{(1)}_{m,c+1\to c}\right]. \tag{59}
$$

We use the $O(1)$ balance equation to eliminate the $\psi^{(1)}$ terms:

$$\bar{B}_{c+} \cdot \bar{J}^{(1)}_{c+1/2} = \sum_{\bar{B}_{c-} \cdot \bar{\Omega}_m > 0} w_m \bar{B}_{c-} \cdot \bar{\Omega}_m \left[ \begin{array}{l} \dfrac{\phi_c^{(1)}}{4\pi} + \dfrac{1}{4\pi} \dfrac{\phi_{c+1}^{(1)} - \phi_c^{(1)}}{2} + T^{(1)}_{m,c\to c+1} \\[2mm] - \dfrac{\bar{\Omega}_m}{\sigma_{t,c} V_c} \cdot \left( \begin{array}{l} \bar{A}_{c+} \psi^{(0)}_{m,c+} + \bar{A}_{c-} \psi^{(0)}_{m,c-} \\ + \bar{B}_{c+} \psi^{(0)}_{m,c+1/2} + \bar{B}_{c-} \psi^{(0)}_{m,c-1/2} \end{array} \right) \end{array} \right]$$

$$+ \sum_{\bar{B}_{c+} \cdot \bar{\Omega}_m < 0} w_m \bar{B}_{c-} \cdot \bar{\Omega}_m \left[ \begin{array}{l} \dfrac{\phi_{c+1}^{(1)}}{4\pi} + \dfrac{1}{4\pi} \dfrac{\phi_c^{(1)} - \phi_{c+1}^{(1)}}{2} + T^{(1)}_{m,c+1\to c} \\[2mm] - \dfrac{\bar{\Omega}_m}{(\sigma_t V)_{c+1}} \cdot \left( \begin{array}{l} \bar{A}_{c+} \psi^{(0)}_{m,c+} + \bar{A}_{c-} \psi^{(0)}_{m,c-} \\ + \bar{B}_{c+1,+} \psi^{(0)}_{m,c+3/2} + \bar{B}_{c+1,-} \psi^{(0)}_{m,c+1/2} \end{array} \right) \end{array} \right]$$

$$= \sum_{\bar{B}_{c-} \cdot \bar{\Omega}_m > 0} w_m \bar{B}_{c+} \cdot \bar{\Omega}_m T^{(1)}_{m,c\to c+1} - \dfrac{\bar{B}_{c+} \cdot}{6\sigma_{t,c} V_c} \left( \bar{B}_{c+} \dfrac{\phi_c^{(0)} + \phi_{c-1}^{(0)}}{2} + \bar{B}_{c-} \dfrac{\phi_c^{(0)} + \phi_{c-1}^{(0)}}{2} \right)$$

$$- \sum_{\bar{B}_{c-} \cdot \underline{\bar{\Omega}_m} > 0} w_m \bar{B}_{c+} \cdot \bar{\Omega}_m \dfrac{\bar{\Omega}_m \cdot}{\sigma_{t,c} V_c} \left( \bar{A}_{c+} \psi^{(0)}_{m,c+} + \bar{A}_{c-} \psi^{(0)}_{m,c-} \right)$$

$$+ \sum_{\bar{B}_{c+} \cdot \bar{\Omega}_m < 0} w_m \bar{B}_{c+} \cdot \bar{\Omega}_m T^{(1)}_{m,c+1\to c} - \dfrac{\bar{B}_{c+} \cdot}{6(\sigma_t V)_{c+1}} \left( \bar{B}_{c+1,+} \dfrac{\phi_{c+1}^{(0)} + \phi_{c+2}^{(0)}}{2} + \bar{B}_{c+1,-} \dfrac{\phi_{c+1}^{(0)} + \phi_c^{(0)}}{2} \right)$$

$$- \sum_{\bar{B}_{c+} \cdot \bar{\Omega}_m < 0} w_m \bar{B}_{c+} \cdot \bar{\Omega}_m \dfrac{\bar{\Omega}_m \cdot}{(\sigma_t V)_{c+1}} \left( \bar{A}_{c+1,+} \psi^{(0)}_{m,c+1,+} + \bar{A}_{c+1,-} \psi^{(0)}_{m,c+1,-} \right). \quad (60)$$

If corners $c$ and $c+1$ are both in the problem interior, each intensity in this equation is isotropic, and the equation reduces to:

$$\bar{B}_{c+} \cdot \bar{J}^{(1)}_{c+1/2} = \sum_{\bar{B}_{t-} \cdot \bar{\Omega}_m > 0} w_m \bar{B}_{c+} \cdot \bar{\Omega}_m T^{(1)}_{m,c\to c+1} + \sum_{\bar{B}_{c+} \cdot \bar{\Omega}_m < 0} w_m \bar{B}_{c+} \cdot \bar{\Omega}_m T^{(1)}_{m,c+1\to c}$$

$$- \dfrac{\bar{B}_{c+} \cdot}{6\sigma_{t,c} V_c} \left( \bar{A}_{c+} \phi_c^{(0)} + \bar{A}_{c-} \phi_c^{(0)} + \bar{B}_{c+} \dfrac{\phi_c^{(0)} + \phi_{c+1}^{(0)}}{2} + \bar{B}_{c-} \dfrac{\phi_c^{(0)} + \phi_{c-1}^{(0)}}{2} \right)$$

$$- \dfrac{\bar{B}_{c+} \cdot}{6(\sigma_t V)_{c+1}} \left( \bar{A}_{c+1,+} \phi_{c+1}^{(0)} + \bar{A}_{c+1,-} \phi_{c+1}^{(0)} + \bar{B}_{c+1,+} \dfrac{\phi_{c+1}^{(0)} + \phi_{c+2}^{(0)}}{2} + \bar{B}_{c+1,-} \dfrac{\phi_{c+1}^{(0)} + \phi_c^{(0)}}{2} \right) \quad (61)$$

If we compare this to Eq. (33), the analogous SCB result, we see that it is identical if we impose the following conditions:

$$T^{(1)}_{m,c\to c+1} = 0 \quad \text{if } c \text{ is interior;} \qquad T^{(1)}_{m,c+1\to c} = 0 \quad \text{if } c+1 \text{ is interior.} \quad (62)$$

Let us summarize our UCB results to this point. The UCB method consists of a conservation equation for each corner, the step closure on cell surfaces, and Eq. (56) on cell-interior corner surfaces. Eq. (56) contains undefined "$T$" terms. If these terms are zero to $O(1)$ and to $O(\varepsilon)$ for interior corners, then the leading-order UCB solution in the interior will satisfy exactly the same equations, Eqs. (29) and (33), as the leading-order SCB solution. Thus, it inherits the strengths and weaknesses of the SCB diffusion-limit discretization.

The remaining unanswered question about the behavior of UCB in thick diffusive problems is the boundary condition satisfied by the leading-order solution. To address this we turn to the tractable case of a rectangular grid. We assume that the opacity $\sigma_t$ is constant across each rectangular cell. In this case several of the dot products in Eq. (60) vanish, others simplify, and two terms cancel. Equation (60) becomes:

$$
\bar{B}_{c+} \cdot \bar{J}^{(1)}_{c+1/2} = \sum_{\bar{B}_{c+} \cdot \bar{\Omega}_m > 0} w_m \bar{B}_{c-} \cdot \bar{\Omega}_m T^{(1)}_{m,c \to c+1} + \sum_{\bar{B}_{c+} \cdot \bar{\Omega}_m < 0} w_m \bar{B}_{c+} \cdot \bar{\Omega}_m T^{(1)}_{m,c+1 \to c}
$$

$$
+ \frac{|B_{c+}|^2}{\sigma_{t,c} V_c} \left[ \sum_{\bar{n}_{c-} \cdot \bar{\Omega}_m < 0} w_m |\bar{n}_{c-} \cdot \bar{\Omega}_m|^2 \psi^{(0)}_{m,c-} - \sum_{\bar{n}_{c+1,+} \cdot \bar{\Omega}_m < 0} w_m |\bar{n}_{c+1,+} \cdot \bar{\Omega}_m|^2 \psi^{(0)}_{m,c+1,+} \right]. \quad (63)
$$

Consider $c$ and $c+1$ such that

$$
\bar{B}_{c+} \cdot \bar{J}^{(1)}_{c+1/2} = \frac{\Delta y_j}{2} J^{N(1)}_{x,1,j}. \tag{64}
$$

That is, consider the two corners $c$ and $c+1$ in the upper half of a cell on the left boundary. We assume that the problem has more than one cell in the $x$ direction, so that the rightmost corner is in the problem interior. Then Eq. (63) is:

$$
\frac{\Delta y_j}{2} J^{N(1)}_{x,1,j} = \sum_{\mu_m > 0} w_m \frac{\Delta y_j}{2} \mu_m T^{N(1)}_{m,1,j,L \to R} + \frac{\Delta y_j}{2} \frac{\sum_{\mu_m > 0} w_m \mu_m^2 \psi^{inc,N}_{m,1/2,j} - \frac{1}{6} \phi^{(0)}_{1/2,j+1/2}}{\sigma_{t,1,j} \Delta x_1}. \quad (65)
$$

Note that if the "$T$" term were zero, we would have a $6\mu^2$-weighted energy density serving as the boundary condition. However, if we define the $T$ term as follows, we will obtain a $(2\mu+3\mu^2)$-weighted boundary condition:

$$
T^N_{m,1,j,L \to R} = \frac{1}{2} \frac{\mu_m \Delta y_j / 2}{\sigma_{t,1,j} \Delta x_i \Delta y_j / 4} \left( \psi^{NW}_{m,1,j} - \psi^N_{m,i-1/2,j} \right)
$$

$$
\xrightarrow[\substack{asymptotic \\ scaling}]{} \varepsilon \frac{1}{2} \frac{\mu_m \Delta y_j / 2}{\sigma_{t,1,j} \Delta x_i \Delta y_j / 4} \left( \psi^{NW}_{m,1,j} - \psi^N_{m,i-1/2,j} \right). \quad (66)
$$

This expression satisfies the conditions we decided upon earlier:

$$T_{m,i,j,L \to R}^{N(0)} = 0,$$  (67a)

$$T_{m,i,j,L \to R}^{N(1)} = \frac{1}{2} \frac{\mu_m \, \Delta y_j / 2}{\sigma_{t,i,j} \, \Delta x_i \Delta y_j / 4} \left( \psi_{m,i,j}^{NW(0)} - \psi_{m,j-1/2,j}^{N(0)} \right)$$  (67b)

$$= \frac{\mu_m}{\sigma_{t,i,j} \Delta x_i} \left( \phi_{i,j}^{NW(0)} - \phi_{i,j}^{NW(0)} \right) = 0 \quad \text{if corner } (ij, NW) \text{ is interior.}$$

If we insert the expression (66) into Eq. (65) we obtain:

$$\frac{\Delta y_j}{2} J_{x,1,j}^{N(1)} = \frac{\Delta y_j}{2} \sum_{\mu_m > 0} w_m \frac{1}{2} \mu_m^2 \frac{\psi_{m,1,j}^{NW(0)} - \psi_{m,1,2,j}^{inc.N}}{\sigma_{t,1,j} \Delta x_1} + \frac{\Delta y_j}{2} \frac{\sum_{\mu_m > 0} w_m \mu_m^2 \psi_{m,1/2,j}^{inc.N} - \frac{1}{6} \phi_{3/2,j+1/2}^{(0)}}{\sigma_{t,ij} \Delta x_1 \Delta y_j}$$

$$= \frac{\Delta y_j}{2} \frac{1}{12 \sigma_{t,1,j} \Delta x_1} \phi_{1,j}^{NW(0)} + \frac{\Delta y_j}{2} \frac{\sum_{\mu_m > 0} w_m \frac{1}{2} \mu_m^2 \psi_{m,1/2,j}^{inc.N} - \frac{1}{6} \phi_{3/2,j+1/2}^{(0)}}{\sigma_{t,ij} \Delta x_1 \Delta y_j}.$$  (68)

We recall from the SCB analysis that the leading-order energy density in a boundary corner is a $4\mu$-weighted integral of an averaged incident intensity:

$$\phi_{1,j}^{NW(0)} = \sum_{\mu_m > 0} w_m 4 \frac{\mu_m}{\rho} \left\langle \psi_{m,1/2,j}^{inc.N} \right\rangle,$$  (69)

and finally we have:

$$\frac{\Delta y_j}{2} J_{x,1,j}^{N(1)} = \frac{\Delta y_j}{2} \left[ \frac{\sum_{\mu_m > 0} w_m \left( 2 \frac{\mu_m}{\rho} \left\langle \psi_{m,1,2,j}^{inc.N} \right\rangle + 3 \mu_m^2 \psi_{m,1/2,j}^{inc.N} \right) - \phi_{3/2,j+1/2}^{(0)}}{6 \sigma_{t,ij} \Delta x_1 \Delta y_j} \right].$$  (70)

This is identical to the SCB result shown in Eq. (48).

We have now constructed an "upstream" corner-balance (UCB) scheme that produces exactly the same leading-order solution as the SCB scheme, at least on rectangular grids. It is relatively easy to generalize our definition (66) to arbitrary grids:

$$T_{m,c \to c+1} = \alpha_{m,c \to c+1} \frac{\vec{A}_{c-} \cdot \vec{\Omega}_m}{\sigma_{t,c} V_c} \left( \psi_{m,c} - \psi_{m,c-} \right)$$

$$\xrightarrow[\substack{asymptotic \\ scaling}]{} \varepsilon \left( \alpha_{m,c \to c+1}^{(0)} + \varepsilon \alpha_{m,c \to c+1}^{(1)} + \cdots \right) \frac{\vec{A}_{c-} \cdot \vec{\Omega}_m}{\sigma_{t,c} V_c} \left( \psi_{m,c} - \psi_{m,c-} \right).$$  (71)

If $\alpha^{(0)}$=1/2, this is identical to Eq. (66) for a rectangular grid. On an arbitrary grid, this does not produce exactly the same boundary condition as SCB; however, it produces essentially the same quality of boundary condition, in that the boundary conditions for both SCB and UCB are averages of a $4\mu$-weighted component and a $6\mu^2$-weighted component. The average will not always be 50-50 for either SCB or UCB.

The "$\alpha$" term in Eq. (71) provides a great deal of flexibility. To obtain the same boundary condition as SCB on rectangles, we need only ensure that $\alpha^{(0)}$=1/2. We can actually *improve* on this boundary condition by choosing $\alpha^{(0)}$=0.455; this leads to the following boundary condition on the left boundary of a rectangular grid:

$$\frac{\Delta y_j}{2} J_{x,1,j}^{N(1)} = \frac{\Delta y_j}{2} \left[ \frac{\sum_{\mu_m>0} w_m \left( 1.82 \frac{\mu_m}{\rho} \left\langle \psi_{m,1/2,j}^{inc,N} \right\rangle + 3.27 \mu_m^2 \psi_{m,1/2,j}^{inc,N} \right) - \phi_{3/2,j+1/2}^{(0)}}{6\sigma_{t,ij}\Delta x_i \Delta y_j} \right] . \quad (72)$$

The $(1.82\mu+3.27\mu^2)$ function is a more accurate approximation of the analytic $W(\mu)$ function than is $(2\mu+3\mu^2)$. Thus, our UCB method is actually an *improved* generalization of the slab-geometry lumped LD method, in that its boundary condition is more accurate. This is not significant except in the case of a grazing-angle incident intensity, in which case the $(1.82\mu+3.27\mu^2)$ function introduces an error of approximately 1% while the $(2\mu+3\mu^2)$ error is more than 10%.

In summary, we have devised an UCB method with the following properties:

- It allows transport sweeps to proceed corner by corner in the direction of particle flow, eliminating the coupling of all corners in a given cell;

- In a thick diffusive problem with a polygonal-cell grid its leading-order interior solution satisfies the same discretized diffusion equation as the leading-order SCB solution;

- Its leading-order solution can solve either the same or an improved boundary condition, relative to SCB's solution, on a rectangular grid. Its boundary condition on arbitrary grids is comparable to SCB's.

- Its closure equation has the flexibility to (perhaps) improve upon the fine- and intermediate-thickness performance of SCB. This

flexibility is contained in the parameter $\alpha$, whose value is prescribed so far only in the thick limit and only to leading order.

In the next subsection we try to exploit the flexibility in $\alpha$ to obtain better performance in regimes other than thick-diffusive.

## C.  Other Limits

Here we shall simply choose $\alpha$ such that the UCB method will have third-order truncation error in the fine-mesh limit, at least for the simple model problem of: slab geometry, $\sigma_r = \sigma_t$, and $S=0$. The work reported in this section was part of a class project performed by K. Thompson at Texas A&M University.[17]

In our model problem, the UCB equations in the $i$th spatial cell for $\mu_m \equiv \Omega_{x,m} > 0$ are:

$$\frac{1}{\tau_{mi}}\left(\psi_{m,i} - \psi_{m,i-1/2}\right) + \psi_{m,i,L} = 0, \qquad \tau_{mi} \equiv \frac{\sigma_{t,i}\Delta x_i}{2|\mu_m|}, \tag{73a}$$

$$\psi_{m,i} = \psi_{m,i,L} + \alpha_{mi}\frac{1}{\tau_{mi}}\left(\psi_{m,i,L} - \psi_{m,i-1/2}\right), \quad \mu_m > 0, \tag{73b}$$

$$\frac{1}{\tau_{mi}}\left(\psi_{m,i+1/2} - \psi_{m,i}\right) + \psi_{m,i,R} = 0, \tag{73c}$$

$$\psi_{m,i+1/2} = \psi_{m,i,R}, \quad \mu_m > 0. \tag{73d}$$

If we solve for the exiting intensity, $\psi_{m,i+1/2}$, in terms of the incident intensity, $\psi_{m,i-1/2}$, we obtain:

$$\psi_{m,i+1/2} = \psi_{m,i-1/2}\frac{\alpha_{mi} + (1 - \alpha_{mi})\tau_{mi}}{\alpha_{mi} + (1 + \alpha_{mi})\tau_{mi} + 2\tau_{mi}^2 + \tau_{mi}^3}. \tag{74}$$

Of course, the exact solution of this problem is

$$\psi_{m,i+1/2} = \psi_{m,i-1/2}e^{-2\tau_{mi}}. \tag{75}$$

We have found an expression for $\alpha_{mi}$ that is a positive monotonic function of $\tau_{mi}$ and yields a fourth-order local truncation error in our simple model problem:

$$\alpha_{mi} = \alpha(\tau_{mi}) = \frac{3 + 4\tau_{mi} + \alpha_0 4\tau_{mi}^2}{2 + 2\tau_{mi} + 4\tau_{mi}^2}. \tag{76}$$

Here the constant $\alpha_0$ is 1/2 if we want the $(2\mu + 3\mu^2)$-weighted boundary condition, or 0.455 if we want the more accurate $(1.82\mu + 3.27\mu^2)$ weighting.

We shall demonstrate in our section on numerical results that UCB with this definition of $\alpha_{ml}$ is significantly more accurate than SCB for problems with thin or intermediate-thickness cells.

To generalize to two dimensions we shall use the same function, Eq. (76), for $\alpha_{m,c \rightarrow c\pm1}$, and simply identify what to use for the argument "$\tau$." We require that if an XY-geometry problem with a rectangular grid has a one-dimensional solution along either $x$ or $y$, the XY UCB method must obtain the one-dimensional UCB solution. We can achieve this with the following definition:

$$\alpha_{m,c \rightarrow c\pm1} = \alpha\left(\tau_{m,c \rightarrow c\pm1}\right) = \alpha\left(\frac{\sigma_{t,c}V_c}{\bar{B}_{c\pm} \cdot \bar{\Omega}_m}\right)$$

$$= \cdots = \frac{3\left(\bar{B}_{c\pm} \cdot \bar{\Omega}_m\right)^2 + 4\bar{B}_{c\pm} \cdot \bar{\Omega}_m \sigma_{t,c}V_c + \alpha_0 4\left(\sigma_{t,c}V_c\right)^2}{2\left(\bar{B}_{c\pm} \cdot \bar{\Omega}_m\right)^2 + 2\bar{B}_{c\pm} \cdot \bar{\Omega}_m \sigma_{t,c}V_c + 4\left(\sigma_{t,c}V_c\right)^2}. \tag{77}$$

In this expression we have multiplied through by $(\bar{B}_{c\pm} \cdot \bar{\Omega}_m)^2$ to avoid numerical difficulties that can arise on arbitrary grids, in which $\bar{B}_{c\pm} \cdot \bar{\Omega}_m$ can be very small or zero. (Note that if $\bar{B}_{c\pm} \cdot \bar{\Omega}_m$ is negative the $\alpha$ parameter is not needed, because the surface is not an outflow surface.)

## V.    ITERATIVE ACCELERATION

The thick diffusive test problems in the next section could not be run without some form of iterative acceleration. For this task we have implemented a preconditioned conjugate gradient (CG) algorithm. Our preconditioning operator consists of a fixed number of transport sweeps on a "low-order" transport problem. The "low-order" transport operator was chosen from the "transport-synthetic acceleration" (TSA) family of Ramoné et al.[18]

Our preconditioned CG algorithm is not extremely efficient, and we certainly do not present it as an ideal iterative method in its current form. However, it was relatively easy to implement and it has enabled us to obtain answers to very difficult test problems in very reasonable times, which is not remotely possible with simple source iteration.

## VI.    NUMERICAL RESULTS

In this section we provide numerical results comparing UCB against SCB and, in some cases, against discontinuous finite-element methods. We begin with

Table 1. Ratio of computed/reference exiting flow rate for Test Problem 1.

| c | $\sigma_t \Delta x = 0.25$ | | $\sigma_t \Delta x = 0.5$ | | $\sigma_t \Delta x = 1$ | |
|---|---|---|---|---|---|---|
| | SCB | UCB | SCB | UCB | SCB | UCB |
| 0.1 | 1.6 | 1.01 | 4.9 | 1.08 | 94 | 2.4 |
| 0.5 | 1.5 | 1.01 | 3.7 | 1.09 | 44 | 2.2 |
| 0.9 | 1.07 | 1.00 | 1.3 | 1.03 | 2.15 | 1.25 |
| 0.99 | 1.00 | 1.00 | 1.01 | 1.00 | 1.03 | 1.02 |

slab geometry and then address XY geometry.

## VI.A.    Slab Geometry

Our first test is a family of deep-penetration problems 50 mean-free paths thick. We include this family of problems to illustrate that UCB is a significant improvement over SCB for problems with thin and intermediate-thickness spatial cells, at least in slab geometry. That is, these problems show that our formulation of the "$\alpha$" in Eq. (73b) does what it was intended to do.

Each problem is a 50-mean-free-path slab with an isotropic intensity incident upon the left surface and no fixed volumetric source. We use a uniform spatial grid and an $S_8$ Gauss-Legendre quadrature set in each problem. We choose various values for the scattering ratio, $c \equiv (\sigma_t - \sigma_r)/\sigma_t$, and the cell thickness, $\sigma_t \Delta x$. For each combination of $c$ and $\sigma_t \Delta x$, we compute the rate of particle outflow at the right surface using SCB and UCB. We report the ratio of computed to reference outflow rates in Table 1. (Reference results were obtained by solving the $S_8$ equations with several methods, including linear discontinuous finite elements. with extremely fine spatial grids.) We see from this table that UCB is indeed far more accurate than SCB, and that it converges more quickly to the correct solution as the mesh is refined.

## VI.B.    XY Test Problems

Our first XY-geometry test problem is actually a sequence of simple problems that become very diffusive. The problem domain is a square 1 cm on each side. Each test problem is characterized by a small parameter $\varepsilon$: the total cross section is $1/\varepsilon$ cm$^{-1}$, the removal cross section is $\varepsilon$ cm$^{-1}$, and the source is $\varepsilon$

particles/cm$^3$-s. As $\varepsilon$ shrinks the problem becomes more optically thick but with lower removal cross section. This problem is designed such that asymptotic diffusion-limit analyses apply to it without question. The analysis of the exact transport equation says the exact solution will approach the diffusion solution as $\varepsilon$ becomes small. The analysis of the bilinear discontinuous (BLD) method on rectangular cells says that the BLD solution on this problem will approach a reasonable discrete approximation of the diffusion solution as $\varepsilon$ gets small, and will thus be accurate.[5] Our analysis of SCB and UCB predicts that each of these methods will also produce accurate solutions as $\varepsilon$ shrinks. In Figure 6 below, we show the bilinear discontinuous (BLD) solution for values of $\varepsilon$ ranging from 0.1 to 0.00001. The figure shows the energy density as a function of $x$ for $y$ fixed at the centerline of the square. As sequence of problems becomes optically thicker with lower removal cross section, the BLD solution clearly approaches a fixed solution, which appears to be diffusion-like. (In fact, we have solved a bilinear continuous discretized diffusion equation for this problem and it does give this fixed solution.) This is not a new result; we include it only for comparison against our SCB and UCB methods.
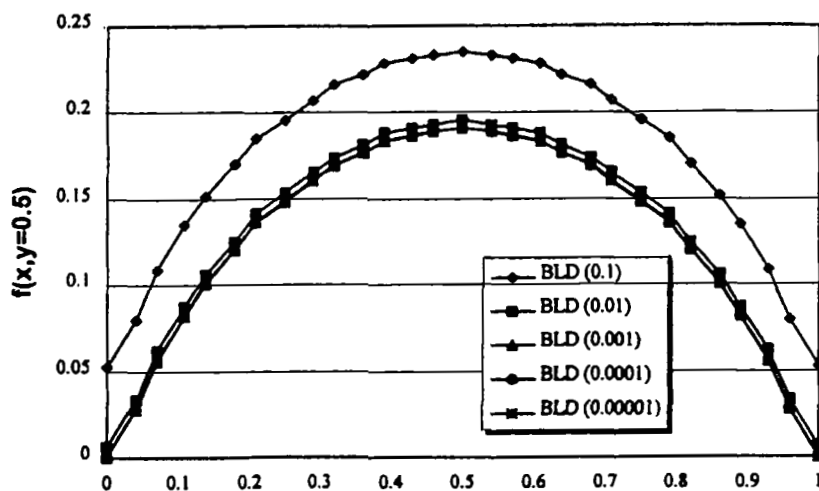


Figure 6. BLD solutions on the line $y=0.5$, as a function of the small parameter $\varepsilon$. The last three plots are essentially coincident.

In Figure 7 we present SCB results for the same sequence of problems. The SCB solution behavior is obviously qualitatively the same as that of the BLD solution, but in numerical detail it is not the same even for the smallest value of $\varepsilon$. This is also predicted by the asymptotic analysis: on a rectangular grid, the BLD solution limits to the solution of a bilinear continuous discretization of the diffusion equation, whereas the SCB and UCB solutions limit to the solution of a five-point finite-difference discretization. Thus, both solutions are reasonable approximations of the exact diffusion solution, but they are not identical.

In Figure 8 we present UCB results for the same sequence of problems. According to our analysis, UCB should achieve exactly the same solution as SCB in the limit as $\varepsilon$ tends to zero. The numerical results confirm this, at least for this simple problem: although the SCB and UCB solutions are different in detail for large $\varepsilon$, they approach each other for small $\varepsilon$.

Our second XY-geometry test problem is designed to examine UCB and SCB for fine and intermediate cell thicknesses. We have already seen that UCB is far more accurate than SCB in one-dimensional problems of this type; we examine it now in two dimensions.

The test problem is a source-free rectangle. 5 × 3 mean-free paths, with an isotropic incident intensity on the left surface. The removal cross section is half of the total. In each problem we used an S4 level-symmetric quadrature set taken from reference.[15] We compute the exiting flow rate from the top right quarter of the problem (that is, exiting flow rate integrated over the right half of the top surface and the top half of the right surface) for various mesh spacings. In Table 2 below we present results from BLD, SCB and UCB. We present BLD results because BLD is a well-known and reasonably accurate method, and thus serves as a known standard against which to compare the others.

Perhaps the most striking result is how poor the SCB solution is. It has large errors for coarser meshes and these errors diminish disappointingly slowly as the mesh is refined. UCB does not suffer from this defect – it is far more accurate than SCB for cells of intermediate and fine thickness, and in fact appears to give approximately the same accuracy as BLD, which is a very strong result. We conclude from these and many other test problems that given rectangular cells of fine or intermediate optical thickness, UCB is a vast improvement over SCB and is roughly comparable to BLD.
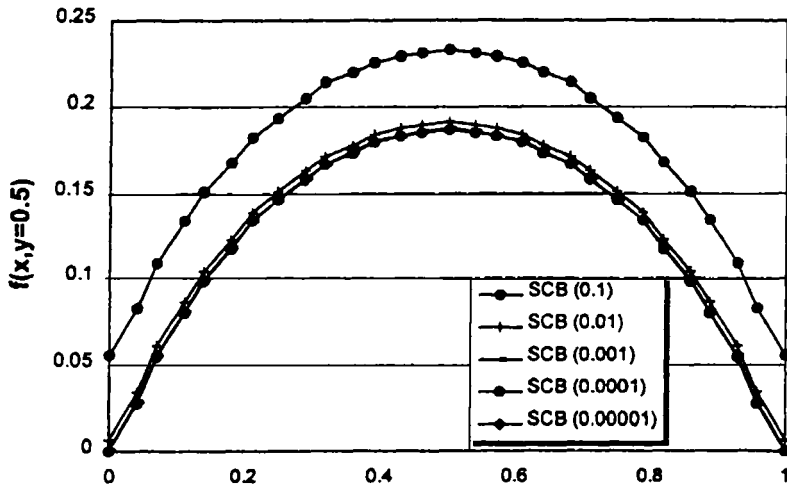
Figure 7.  SCB solutions on the line y=0.5, as a function of the small parameter $\varepsilon$.
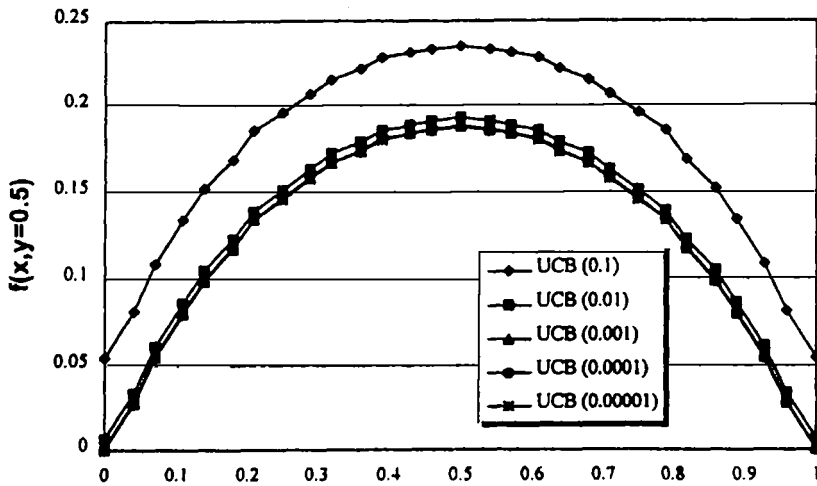The last three plots are essentially coincident.



Figure 8.  UCB solutions on the line y=0.5, as a function of the small parameter $\varepsilon$.
The last three plots are essentially coincident.

Table 2.  Exiting flow rate from XY test problem.

| number of | Method | | |
|:---:|:---:|:---:|:---:|
| cells | BLD | SCB | UCB |
| 2 × 2 | -0.011227 | 0.074538 | 0.050435 |
| 4 × 4 | 0.023042 | 0.041668 | 0.029538 |
| 8 × 8 | 0.025804 | 0.030830 | 0.026347 |
| 16 × 16 | 0.025982 | 0.027441 | 0.025967 |
| 32 × 32 | 0.026034 | 0.026427 | 0.026049 |
| 64 × 64 | 0.026040 | 0.026143 | 0.026037 |

Our third XY-geometry test problem is designed to expose weaknesses in spatial-discretization methods.  It contains optically thick absorbing regions, a near vacuum, and an optically thick diffusive region.  The optically thick diffusive region contains a boundary layer.  We impose a very coarse mesh, as shown in Figure 9.  Most transport discretizations will produce negative solutions in some regions of this problem; those that do not are still likely to produce large errors. Particles are born in the leftmost region: many are absorbed in the adjacent absorbing region; some stream through the optically thin region at the bottom. Some of the particles that stream through will be absorbed in the very thick absorbing region at the bottom right; some will be incident at grazing angles on the very thick diffusive region in the upper right.  This introduces a boundary layer in the that region, which is not resolved by the very coarse spatial grid we impose on the problem.

In Figure 10 we present the BLD solution of this test problem.  The figure shows logarithmically spaced contours of the solution. ranging from $10^1$ to $10^{-16}$ in increments of $10^{0.2}$.  The solution is highest in the left (source) region, and decreases to the right.  White space indicates a negative solution.  This problem illustrates the main drawbacks of BLD for radiative transfer.  The BLD solution is not monotonic in the thick absorber regions, but oscillates between negative and positive.  In the thick diffusive region the solution is not as smooth as it should be, especially near the boundary layer, and the solution is negative even in portions of this region.

In Figure 11 we present the solution from the BLD method with mass-matrix lumping[15] – the lumped BLD (LBLD) solution.  We see that lumping has added
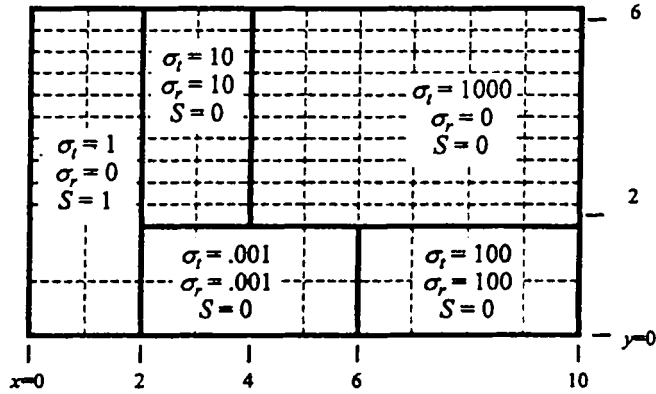
Figure 9. Difficult XY test problem. Spatial grid is shown as dotted line. All boundaries are vacuum.
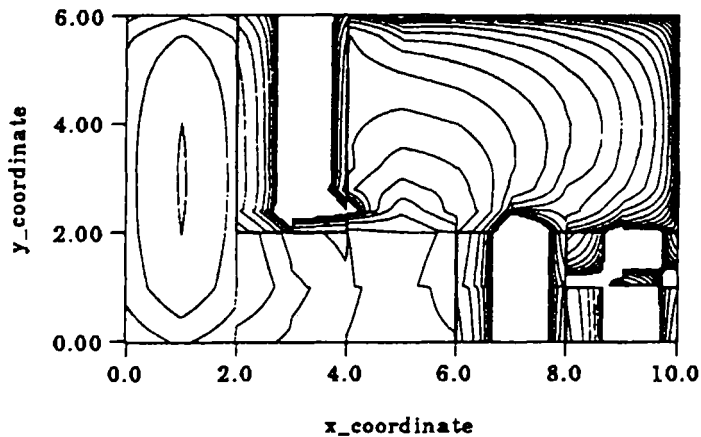


Figure 10. Logarithmically spaced contours of BLD solution, Test Problem 3.

robustness to the method, as it typically does to finite-element schemes – the solution is now positive in and near the first absorbing region. However, the solution is still not as smooth as it should be in the thick diffusive region, and it is still negative in portions of that region and in the strongest absorber. This method is an improvement over BLD, but it remains far from perfect.
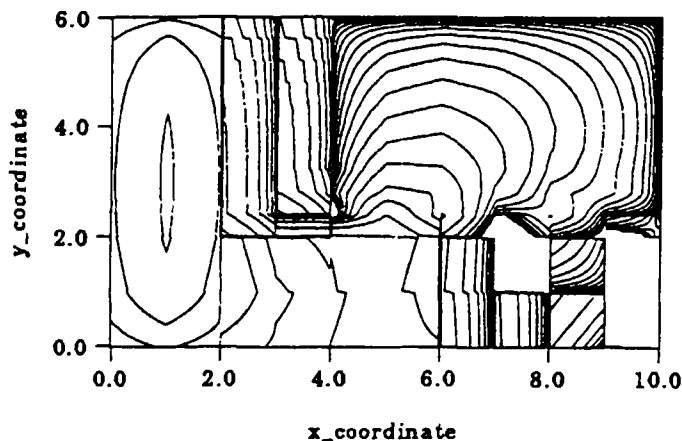
Figure 11. Logarithmically spaced contours of LBLD solution, Test Problem 3.

In Figure 12 we present the SCB solution of the same problem. We note first that the solution is everywhere positive and monotonic. In addition, SCB obtains what appears to be a reasonable discrete diffusion solution in the thick diffusive region. In spite of the difficulty of the problem and the coarseness of the grid, the SCB method yields a solution that is true to the physics of the problem in many important respects: it is positive, monotonic, and believable in the diffusive region. We do not claim that the SCB solution on such a coarse grid is very accurate in this problem; our point is that it reproduces the correct physical trends. This is a highly desirable characteristic of any method that will be used in the design and analysis of complex systems, and it is not easy to achieve.

In Figure 13 we present the UCB solution of the same problem. We note first that the UCB solution is negative in a small portion of the thin region and also in part of the thickest absorbing region. The origin of this negativity is the thin region, not the thick one. The basic problem is that UCB assumes some degree of smoothness in the solution across a given cell; this is how it achieves higher fine-mesh accuracy. In the thin region of this problem, the intensity in a given direction is discontinuous or nearly so, and UCB basically extrapolates to a negative value. There are more signs of this trouble in the non-monotonic behavior in the thin region. However, if we examine the absorbing regions and
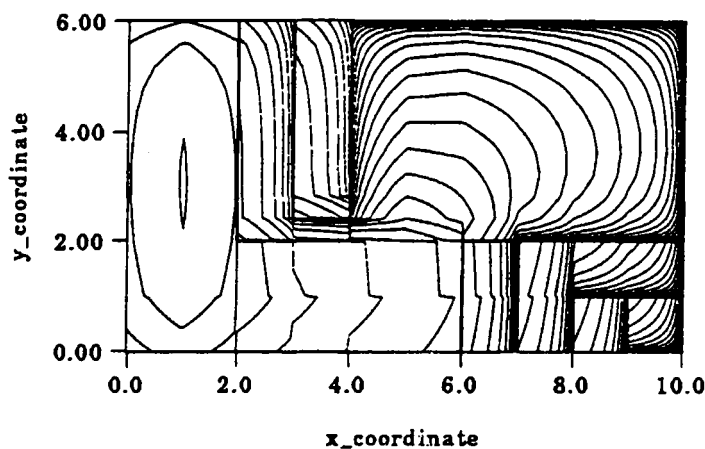
Figure 12.  Logarithmically spaced contours of SCB solution, Test Problem 3.
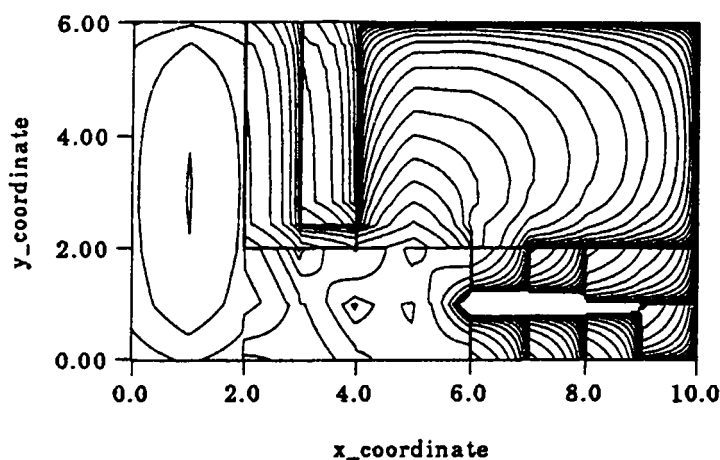


Figure 13.  Logarithmically spaced contours of UCB solution, Test Problem 3.

the diffusive region, we find behavior very similar to SCB, which is highly desirable.

In summary, our numerical tests demonstrate several characteristics of our new UCB scheme.  First, in thick diffusive regions it behaves like SCB, as it was

designed to do. Second, on meshes of fine and intermediate thickness, UCB is far more accurate than SCB and actually achieves accuracy comparable to the BLD scheme. These are highly desirable characteristics. However, we also find that UCB is susceptible to oscillations and negative solutions given streaming through a void or near-void. At this point we accept this as the price we pay for the more accurate fine-mesh limit, but we will discuss this further in the next section.

The UCB method discussed here was designed with arbitrary spatial grids in mind, and we have implemented it for the general case of an arbitrarily connected grid of polygons. We have tested it extensively with grids that are mixtures of triangles and quadrilaterals. Our experience is that when cells are not very distorted, the solution in diffusive regions is roughly independent of the grid, which is a desirable property. However, we do notice some degradation in the solution, as predicted by our asymptotic analysis, for cells that are distorted. We discuss this further in the next section.

## VII.   CONCLUSIONS

We have introduced a new spatial discretization method for two-dimensional radiative transfer problems. The method, which we call "upstream" corner balance (UCB), has its origins in a previous method called "simple" corner balance (SCB). Both methods are designed for use on grids of arbitrarily connected polygons, and both impose particle conservation ("balance") on quadrilateral subcells that we call "corners." However, an SCB calculation of the angular intensity with a given total source requires the inversion of an N×N system of equations in each N-sided polygonal cell, whereas the UCB calculation can proceed one subcell at a time. This makes UCB far easier to implement for truly arbitrary grids, and also makes it computationally less expensive to run.

In this paper we have presented an asymptotic analysis of the SCB solution in thick diffusive regions with arbitrary spatial grids. This complete analysis has not been published before. The analysis predicts excellent behavior on rectangular cells: the leading-order interior solution satisfies a standard five-point diffusion discretization, with boundary conditions that very closely match the ideal conditions even when sharp boundary layers are not resolved by the spatial grid. To our knowledge, SCB was the first method to achieve this desirable property. We designed UCB such that its solution limits to the SCB solution in thick

diffusive regions; thus, it also achieves excellent performance in thick diffusive problems with rectangular cells, even with unresolved boundary layers. To our knowledge, UCB and SCB remain the only published methods with this property. However, a careful study of the results of our asymptotic analysis indicates that the SCB solution can degrade in thick diffusive problems with distorted polygonal cells; UCB inherits this flaw. We have observed this degradation in numerical calculations using UCB, although we have not provided numerical results in this paper. It is difficult to design a transport discretization with accurate "diffusion-limit" behavior on distorted grids, in large part because it is not clear what an accurate diffusion discretization might be on such grids. There has been considerable recent work toward developing accurate diffusion discretizations for distorted grids, however, and we expect such work to guide the development of transport discretizations that will have more accurate and robust behavior for diffusive problems on such grids. Meanwhile, we note that the degradation of SCB and UCB on distorted grids can be traced at least partially to the fact that they do not exactly capture an energy density that is a linear function of position. (They do so on rectangular cells.) We have now developed a new UCB method that exactly captures linear solutions regardless of the grid, and we are in the process of implementing and testing it. Our analysis predicts that it will behave extremely well in diffusive regions, independent of the grid. We expect to report on this in the near future; in that report we will include many problems with non-rectangular cells, thus filling a gap left by this paper.

The analysis and results presented in this paper consider a very simple version of a radiative-transfer problem: a one-group (or "grey") steady-state equation with opacities that are assumed to be given (instead of depending on temperature and thus on the solution). A fair question is whether this has any bearing on practical problems, which are often time-dependent, frequency-dependent, and nonlinear. We offer several answers. First, our experience to date has been that if a spatial discretization method performs well on the steady-state problems analyzed here, it also performs well on realistic problems. Second, we have implemented UCB (in collaboration with Paul Nowak) in a radiative-transfer code and tested it on nonlinear time-dependent multi-frequency problems; it performs exactly as one would expect based on its performance in the problems presented here. Third, we have analyzed and tested (also in collaboration with

Paul Nowak) SCB for time-dependent, multi-frequency, nonlinear radiative transfer problems; results will be reported in reference 8. The basic conclusion of that work, which is limited to one spatial dimension, is that SCB performs essentially as well on such problems as it does on linear one-group steady-state problems. The UCB method presented here will inherit that performance. (In reference 7 Morel et al. analyze a very similar scheme for a similar problem and reach similar conclusions.)

The SCB scheme is known to produce poor solutions given spatial cells of thin or intermediate optical thickness. We have designed our UCB scheme to not only permit subcell-by-subcell sweeping through the mesh, but also to generate vastly improved solutions on thin and intermediate cells. Our numerical results clearly demonstrate that this is the case: when the solution is smooth, UCB appears to generate fine- and intermediate-mesh results that are comparable to the well-known bilinear discontinuous (BLD) finite-element method. However, at the price we pay for this higher-order accuracy in the present version of UCB is that it can be susceptible to oscillations and negative solutions in streaming-dominated regions. In our new UCB method, mentioned above, we attempt to rectify this problem. Despite this flaw, our tests to date indicate that UCB is a better choice than either SCB or BLD for general radiative-transfer problems.

## ACKNOWLEDGMENTS

# REFERENCES

1.  E.W. Larsen, G.C. Pomraning, V.C. Badham, "Asymptotic Analysis of Radiative Transfer Problems," *JQSRT* 29, p. 285 (1983).

2.  E.W. Larsen, J.E. Morel, and W.F. Miller, Jr., "Asymptotic Solutions of Numerical Transport Problems in Optically Thick, Diffusive Regimes." *J. Comput. Physics* 69, p. 283 (1987).

3.  E.W. Larsen and J.E. Morel, "Asymptotic Solutions of Numerical Transport Problems in Optically Thick, Diffusive Regimes II," *J. Comput. Physics* 83, p. 212 (1989). See also "Corrigendum," *J. Comput. Physics* 91, p. 246 (1990).

4.  M.L. Adams, "Even-Parity Finite-Element Transport Methods in the Diffusion Limit," *Progress in Nuclear Energy* 25, No. 2-3, 159-198 (1991).

5.  M.L. Adams, "Discontinuous Finite-Element Transport Solutions in the Thick Diffusion Limit in Cartesian Geometry," *Proc. International Topical Mtg. on Advances in Mathematics, Computations, and Reactor Physics*, vol. 5, p. 21.1 3-1 (1991).

6.  E.W. Larsen, "The Asymptotic Diffusion Limit of Discretized Transport Problems," *Nucl. Sci. Eng.* 112, 336 (1992).

7.  J.E. Morel, T.A. Wareing, and K. Smith, "A Linear Discontinuous Spatial Differencing Scheme for $S_N$ Radiative Transfer Calculations," *J. Comput. Physics* 128, No. 2, pp. 445-462 (1996).

8.  M.L. Adams and P.F. Nowak, "Asymptotic Analysis of Continuous and Discrete Radiative Transfer Problems," in preparation. See also M.L. Adams, E.W. Larsen, and P.F. Nowak, "The Asymptotic Diffusion Limit of Continuous and Discrete Steady-State Multigroup Radiative Transfer Problems," *Proc. Int. Conf. Advances in Mathematics and Computation, Reactor Physics, and Environmental Analysis*, Portland, OR, April 30-May 4, Vol. 1, p. 360 (1995).

9.  M.L. Adams, T.A. Wareing, and W.F. Walters, "Characteristic Methods in Thick Diffusive Problems," *Nucl. Sci. Eng.*, submitted (1997).

10. G.C. Pomraning, The Equations of Radiation Hydrodynamics, Pergamon Press, Oxford (1973).

11. F. Malgavi and G.C. Pomraning, "Initial and Boundary Conditions for Diffusive Linear Transport Problems," *J. Math. Physics* 32, 805 (1990).

12. S. Chandrasekhar, Radiative Transfer, Dover, New York (1960).

13. J.E. Morel and E.W. Larsen, "A Multiple Balance Approach for Differencing the $S_N$ Equations," *Nucl. Sci. Eng* 105, p. 1 (1990).

14. C. Börgers, E.W. Larsen, and M.L. Adams, "The Asymptotic Diffusion Limit of a Linear Discontinuous Discretization of a Two-Dimensional Linear Transport Equation," *J. Comput. Physics* 98, p. 285 (1992).

15. T.A. Wareing, E.W. Larsen, and M.L. Adams, "Diffusion Accelerated Discontinuous Finite Element Schemes for the $S_N$ Equations in Slab and XY geometries." *Proc. International Topical Mtg. on Advances in Mathematics, Computations, and Reactor Physics,* Vol 3, section 11.1, p. 2-1 (1991).

16. T.L. Eaton and M.L. Adams, "A New Corner-Balance/Linear-Discontinuous Method for Transport in Slab Geometry," *Trans. Am. Nucl. Soc.* **70**, p. 158-159 (1994).

17. K. Thompson, private communication (1995).

18. G.L. Ramoné, M.L. Adams, and P.F. Nowak. "A Transport-Synthetic Acceleration Method for Transport Iterations." *Nucl. Sci. Eng.*, **125** pp. 257-283 (1997).